

IMPROVING NON-CONSTANT LUMINANCE COLOR ENCODING EFFICIENCY FOR  
HIGH DYNAMIC RANGE VIDEO APPLICATIONS

by

Fujun Xie

BS in Electrical Engineering, Georgia Institute of Technology, 2014

A THESIS SUBMITTED IN PARTIAL FULFILLMENT OF THE REQUIREMENTS FOR THE  
DEGREE OF

MASTER OF APPLIED SCIENCE

in

The Faculty of Graduate and Postdoctoral Studies

(Electrical and Computer Engineering)

THE UNIVERSITY OF BRITISH COLUMBIA

(Vancouver)

June 2017

© Fujun Xie, 2017

## **Abstract**

Non-Constant Luminance (NCL) and Constant Luminance (CL) are the two common methods for converting RGB values to luma and chroma for compression efficiency. CL coefficients have been derived from the luminous efficacy of the used gamut color primaries in the light linear domain. NCL applies the same coefficients but on non-linear inputs, which are perceptually encoded values using proper transfer function, thus leading to reduced compression efficiency and color shifts. However, since legacy cameras capture perceptually encoded values of light, it is common practice to use NCL in the existing video distribution pipelines. Although color distortion was not a serious problem with legacy Standard Dynamic Range (SDR) systems, this is not the case with High Dynamic Range (HDR) applications where color shifts become much more visible and prohibitive to delivering high quality HDR.

In this thesis, we propose methods that address the inefficiencies of the conventional NCL method by optimizing NCL luma values to be as close as possible to those of CL, thus improving compression performance and color accuracy, while maintaining the current pipeline infrastructure. First, we develop a global optimization method for deriving new optimum coefficients that approximate NCL values to those of the CL approach. Then, we improve upon this approach by conducting content based optimization. This adaptive optimization method takes content pixel density into consideration and optimizes only based on these color distributions. Finally, we propose a weighted global optimization method, which separates chromaticity into three categories (Red, Green, and Blue), and assigns weights based on their contributions to luminance. Evaluations show that the proposed method improves color quality and compression efficiency over NCL.

## **Lay Summary**

Colors are represented with RGB values, where each color has three channels, Red, Green, and Blue. For efficient transmission, RGB inputs are converted to one luminance and two color values to take advantage of the fact that human eyes are more sensitive to luminance than color. During compression, the color portion is filtered without affecting the overall visual quality. However, the original conversion from RGB to luma and chroma signals introduces color shifts and visual artifacts. Although these may not be problematic for existing Standard Dynamic Range systems, they are prohibitive in the case of the emerging High Dynamic Range applications. In this thesis, we developed methods that improve color accuracy and compression efficiency, paving the path for delivering high quality High Dynamic Range services, while using the existing pipeline infrastructure.

## **Preface**

All of the work presented here in this thesis was conducted in the Digital Multimedia Laboratory at the University of British Columbia, Vancouver campus.

A version of Chapter 3 has been published as F. Xie, R. Boitard, M. T. Pourazad, and P. Nasiopoulos, “Optimizing non constant luminance into constant luminance for high dynamic range video distribution,” in IEEE International Conference on Acoustics, Speech and Signal Processing (ICASSP), New Orleans, USA, March 2017. I was the lead investigator responsible for all areas of research, data collection, and the majority of manuscript composition. R. Boitard and M. T. Pourazad were involved in the early stages of research concept formation and aided with manuscript edits. P. Nasiopoulos was the supervisor on this project and was involved with research concept formation, and manuscript edits.

A version of Chapter 4 is submitted to The Digital Media Industry and Academic Forum Conference as F. Xie, M. Azimi, R. Boitard, M. T. Pourazad, and P. Nasiopoulos, “Adaptive optimization of non-constant luminance to constant luminance for hdr video distribution.” I was the lead investigator responsible for all areas of research, data collection, as well as the manuscript edit. M. Azimi and R. Boitard were involved in research concept formation. M. T. Pourazad was involved in the early stages of research concept formation and aided with manuscript edits. P. Nasiopoulos was the supervisor on this project and was involved with research concept formation, and manuscript edits.

A version of Chapter 5 is planning to be submitted to an IEEE Journal as F. Xie, M. Azimi, R. Boitard, M. T. Pourazad, and P. Nasiopoulos, “Weighted global optimization of non-constant luminance to constant luminance for hdr video distribution.” I was the lead investigator responsible for all areas of research, data collection, as well as the manuscript composition. M. Azimi was involved in research concept formation, data collection and implementation. R. Boitard was involved in the early research concept formation. M. T. Pourazad was involved in the early stages of research concept formation and aided with manuscript edits. P. Nasiopoulos was the supervisor on this project and was involved with research concept formation, and manuscript edits.

# Table of Contents

<b>Abstract</b> .....	<b>ii</b>
<b>Lay Summary</b> .....	<b>iii</b>
<b>Preface</b> .....	<b>iv</b>
<b>Table of Contents</b> .....	<b>vi</b>
<b>List of Tables</b> .....	<b>viii</b>
<b>List of Figures</b> .....	<b>ix</b>
<b>List of Abbreviations</b> .....	<b>xii</b>
<b>Acknowledgements</b> .....	<b>xiii</b>
<b>Dedication</b> .....	<b>xiv</b>
<b>1 Introduction</b> .....	<b>1</b>
1.1 Motivation.....	3
1.2 Thesis Organization.....	4
<b>2 Background</b> .....	<b>5</b>
2.1 High Dynamic Range (HDR) Technology.....	5
2.2 Perceptual Encoding.....	8
2.3 High Dynamic Range (HDR) Transmission Pipeline.....	10
2.4 Color Encoding.....	10
2.5 Luma Adjustment.....	13
<b>3 Global Optimization of Non Constant Luminance (NCL) to Constant Luminance (CL) for High Dynamic Range (HDR) Video Distribution</b> .....	<b>16</b>
3.1 Introduction.....	16
3.2 Proposed Method.....	16

3.3 Results and Discussions .....	18
3.4 Conclusion.....	21
<b>4 Content Adaptive Optimization of Non Constant Luminance (NCL) to Constant Luminance (CL) for High Dynamic Range (HDR) Video Distribution.....</b>	<b>23</b>
4.1 Introduction .....	23
4.2 Our Method .....	23
4.3 Experiment Setup.....	25
4.4 Results and Discussions .....	26
4.5 Conclusion.....	32
<b>5 Weighted Global Optimization of Non Constant Luminance (NCL) to Constant Luminance (CL) for High Dynamic Range (HDR) Video Distribution.....</b>	<b>34</b>
5.1 Introduction .....	34
5.2 Our Proposed Method .....	35
5.3 Experiment Setup.....	39
5.4 Results and Discussions .....	42
5.5 Conclusion.....	59
<b>6 Conclusion and Future Work.....</b>	<b>61</b>
6.1 Conclusion.....	61
6.2 Future Work .....	62
<b>Bibliography .....</b>	<b>64</b>

## List of Tables

Table 3.1: Comparison between our NCL ( $Y_a'$ ) and original NCL ( $Y_n'$ ) with CL ( $Y_c'$ ) over all possible 10-bit RGB combinations .....	18
Table 3.2: Average BD-rate reduction under the same visual and color quality .....	19
Table 4.1: New derived coefficients for contents .....	25
Table 4.2: Applied QPs for each content .....	26
Table 4.3: Average BD-rate reduction under the same color quality .....	26
Table 5.1: Visible color wavelength range .....	36
Table 5.2: HDR video dataset .....	40
Table 5.3: Applied QPs for each content .....	41
Table 5.4: Average BD-rate reduction under same visual and color quality .....	42
Table 5.5: Max and average CIEDE2000 values for NCL and our method at each luminance levels .....	58
Table 5.6: Percentage of CIEDE2000 values less than one for NCL and our method at each luminance level .....	59

## List of Figures

Figure 1.1. Chromaticity diagram with BT.709 and BT.2020 color gamut.....	2
Figure 2.1. The dynamic range of real world scenes and capabilities of the human eye, camera, and display .....	5
Figure 2.2. Comparison between (a) an SDR image and (b) an HDR tone-mapped image .....	7
Figure 2.3. Human eyes and cameras' responses for light .....	8
Figure 2.4. Quantization for linear encoded and perceptually encoded signals .....	9
Figure 2.5. General workflow of an HDR transmission pipeline .....	10
Figure 2.6. Workflows of NCL (top), and CL (bottom) encoding methods.....	11
Figure 2.7. PQ transfer function has steep slope at luminance values close to 0 .....	14
Figure 2.8. Workflow of luma adjustment.....	15
Figure 3.1. Chromaticity distribution for the first frame of the FireEater2 sequence in CIE 1931 color space .....	20
Figure 3.2. Chromaticity distribution for the first frame of the SunRise sequence in CIE 1931 color space .....	20
Figure 4.1. Chromaticity distribution for the first frame of the Tibul2 sequence in CIE 1931 color space.....	27
Figure 4.2. Chromaticity distribution for the first frame of the BalloonFestival sequence in CIE 1931 color space .....	28

Figure 4.3. Chromaticity distribution for the first frame of the Market3 sequence in CIE 1931 color space .....	28
Figure 4.4. Chromaticity distribution for the first frame of the Hurdles sequence in CIE 1931 color space .....	29
Figure 4.5. DE100 vs bit-rate for FireEater2 .....	30
Figure 4.6. DE100 vs bit-rate for BalloonFestival .....	31
Figure 4.7. DE100 vs bit-rate for Market3 .....	31
Figure 4.8. DE100 vs bit-rate for Hurdles .....	32
Figure 5.1. CIE 1931 xy chromaticity diagram with BT.2020 gamut coverage.....	35
Figure 5.2. The full visible color spectrum and associated wavelength .....	36
Figure 5.3. Enhanced CIE 1931 xy chromaticity diagram with divisions for different colors .....	37
Figure 5.4. Separation of CIE 1931 xy chromaticity diagram into Red, Green, and Blue .....	38
Figure 5.5. tOSNR-XYZ vs bit-rate for FireEater2 .....	43
Figure 5.6. tOSNR-XYZ vs bit-rate for Market3 .....	44
Figure 5.7. tOSNR-XYZ vs bit-rate for SunRise .....	44
Figure 5.8. tOSNR-XYZ vs bit-rate for Hurdles .....	45
Figure 5.9. De100 vs bit-rate for FireEater2 .....	45
Figure 5.10. DE100 vs bit-rate for Market3 .....	46
Figure 5.11. De100 vs bit-rate for SunRise .....	46
Figure 5.12. DE100 vs bit-rate for Hurdles .....	47

Figure 5.13. Color difference experiment workflow .....	47
Figure 5.14. Color distortion at different luminance levels (0.005 to 0.1 cd/m <sup>2</sup> ) for 10-bit NCL Yn'CBCR with PQ transfer function .....	50
Figure 5.15. Color distortion at different luminance levels (0.005 to 0.1 cd/m <sup>2</sup> ) for 10-bit our proposed Ya'CBCR with PQ transfer function .....	51
Figure 5.16. Color distortion at different luminance levels (1 to 50 cd/m <sup>2</sup> ) for 10-bit NCL Yn'CBCR with PQ transfer function .....	52
Figure 5.17. Color distortion at different luminance levels (1 to 50 cd/m <sup>2</sup> ) for 10-bit our proposed Ya'CBCR with PQ transfer function .....	53
Figure 5.18. Color distortion at different luminance levels (100 to 1000 cd/m <sup>2</sup> ) for 10-bit NCL Yn'CBCR with PQ transfer function .....	54
Figure 5.19. Color distortion at different luminance levels (100 to 1000 cd/m <sup>2</sup> ) for 10-bit our proposed Ya'CBCR with PQ transfer function .....	55
Figure 5.20. Color distortion at different luminance levels (5000 and 10000 cd/m <sup>2</sup> ) for 10-bit NCL Yn'CBCR with PQ transfer function .....	56
Figure 5.21. Color distortion at different luminance levels (5000 and 10000 cd/m <sup>2</sup> ) for 10-bit our proposed Ya'CBCR with PQ transfer function .....	57

## List of Abbreviations

AVC	Advanced Video Coding
BD	Bjontegaard's Delta
CIE	Commission Internationale del'Eclairage
CL	Constant Luminance
CfE	Call for Evidence
CRT	Cathode Ray Tube
cd/m <sup>2</sup>	Candela Per Square Meter
fps	Frames Per Second
HDR	High Dynamic Range
HEVC	High Efficiency Video Coding
HVS	Human Visual System
ITU-T	International Telegraph Union-Telecommunication Standardization Sector
JND	Just Noticeable Difference
MPEG	Motion Picture Experts Group
NCL	Non Constant Luminance
PQ	Perceptual Quantizer
PSNR	Peak Signal-to-Noise Ratio
QP	Quantization Parameter
SDR	Standard Dynamic Range
SMPTE	Society of Motion Picture and Television Engineers
TMO	Tone Mapping Operators
WCG	Wide Color Gamut

## **Acknowledgements**

I would like to start by expressing my most sincere gratitude to my supervisor and mentor **Dr. Panos Nasiopoulos** for his support through the past three years and patient guidance and inspiration through the thesis.

I would also like to thank **Dr. Mahsa T. Pourazad** for her constant help and support during different stages of this thesis.

I am also grateful to my lab mates, **Dr. Ronan Boitard**, and **Maryam Azimi**, who helped me thorough feedback and support during different stages of my research.

My utmost gratitude to my beloved **parents**, who always believed in me and encouraged me through my whole life. I am always thankful to their unconditional love, unlimited dedication, and all the sacrifices they made for me. Without them, I will never be who I am today.

## **Dedication**

To my beloved family

## 1 Introduction

As a new emerging technology with exciting potential, High Dynamic Range (HDR) technology has attracted the attention of consumers, camera and display manufacturers, and broadcasters [1]. Although HDR was first introduced in some conceptual form more than two decades ago [2], it is only just recently that started to mature as technology. The increasing availability of some entry level HDR displays in the consumer market, along with the advances in camera technologies [3], will soon empower broadcasting companies to offer HDR video services.

HDR technology can capture and represent the full range of perceptible shadow and highlight information, offering real life visual quality, close to that perceived by the human eye [1]. HDR values correspond to floating point physical light intensities measured in candela per square meter ( $\text{cd/m}^2$ ) or nits. When HDR content is shown on a HDR display, viewers can potentially view the entire range of perceptible color and brightness. Standard Dynamic Range (SDR) technology, on the other hand, represents integer code values, which correspond to relative light intensities [4]. Furthermore, with limited dynamic range and color gamut, SDR can capture and reproduce only part of the luminance range and visible color information. More specifically, HDR can cover luminance range from 0.005 to 10,000  $\text{cd/m}^2$ , while the SDR technology can only handle a luminance range from 0.1 to 100  $\text{cd/m}^2$ . Regarding color, HDR covers the color gamut range defined by BT.2020 recommendation [5] while SDR covers the limited color gamut defined by the BT.709 recommendation [6] (please see Fig. 1.1). These limitations in the case of SDR are imposed by both the capturing and displaying technologies and the way pixels are represented throughout the traditional distribution pipeline.

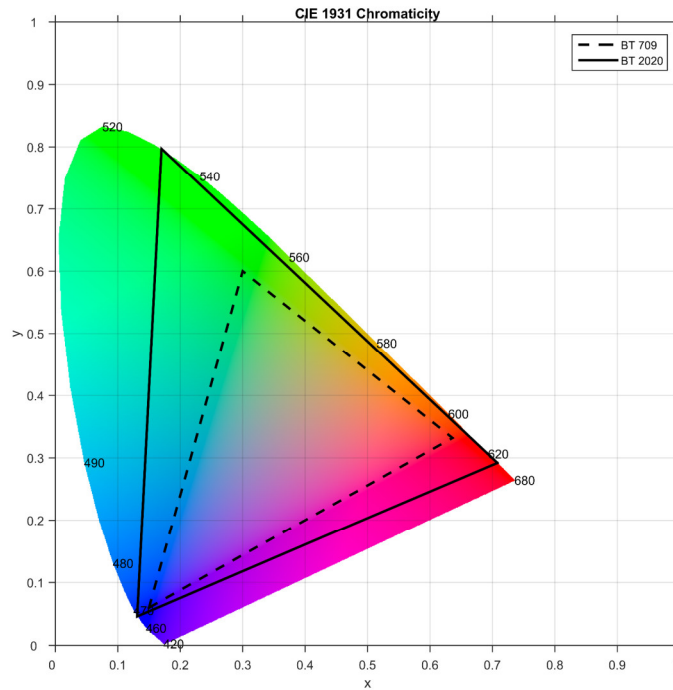


**Figure 1.1. Chromaticity diagram with BT.709 and BT.2020 color gamut**

In general, SDR and HDR video content is captured in Red, Green, and Blue (RGB) format, where each pixel is represented with three color channels (R, G, and B). When transmitting SDR/HDR sequences, pixels are traditionally decomposed into a luma ( $Y'$ ) -chroma (color) signal format for improved compression efficiency. Such a representation separates light from color information thus improving decorrelation between the light and chroma channels. Since the human eyes are more sensitive to luminance change than chrominance change, chroma signals can be filtered with minimum impact on visual quality [7]. This filtering is known as chroma down-sampling, which reduces the amount of information to encode and thus the bitrate for color signals with little to no degradation on perceptual quality [8]. Compression efficiency is therefore improved.

To convert Red, Green, and Blue (RGB) values into a luma and two chroma format, such

as  $Y'CbCr$ , two methods are usually considered: Non-Constant Luminance (NCL) and Constant Luminance (CL). In the case of CL, luminance is calculated as a linear combination of the R, G, and B colors, with the corresponding weighted coefficients derived using a color matching experiment with linearly generated RGB values [9]. The NCL method applies the same weighting coefficients on non-linear RGB values which are perceptually encoded using either gamma or a perceptual quantizer (denoted  $R'G'B'$  in this paper) [10] [11]. Since these weighting coefficients were derived for the CL case with light linear RGB inputs, using the same coefficients in the NCL method results in reduced compression efficiency and color distortions, as detailed in the ITU-R Recommendation BT.2246 [8]. However, given the fact that legacy cameras generate non-linear perceptually encoded content, it is common practice to follow the NCL implementation in the existing SDR content delivery pipelines despite its compression and visual quality drawbacks [8].

Color distortion was not a serious problem with legacy SDR systems, because SDR has limited dynamic range and smaller color gamut than what the human eyes can perceive in the real world. With the introduction of HDR and Wide Color Gamut (WCG), however, these color shifts become much more visible and prohibitive to delivering high quality HDR. Despite the importance of color accuracy in HDR and the compression inefficiency of NCL, broadcasters and display manufacturers continue to support the NCL approach for the time being. This is due to the simplicity of the NCL implementation and the fact the CL implementation radically diverts from the existing display infrastructure [12].

## **1.1 Motivation**

Since compression efficiency and visual quality are of paramount importance in the case

of HDR, finding a way of improving the performance of NCL to the levels offered by CL has become a hot topic of research. In this thesis, we focus on HDR distribution and address the inefficiencies of the conventional NCL method by optimizing NCL luma values to be as close as possible to those of CL, thus improving compression performance and color accuracy, while maintaining the current pipeline infrastructure.

## **1.2 Thesis Organization**

The rest of the thesis is structured as follows. Chapter 2 provides background information and comparison between NCL and CL. Chapter 3 explains in detail our first proposed global optimization method for NCL. In Chapter 4, we improve upon our first approach by developing a new, local, content adaptive optimization method. Chapter 5 presents our weighted global optimization method, which turns out to be the most effective method for approximating NCL values to those of CL. Finally, conclusions, discussions and future work are drawn in Chapter 6.

## 2 Background

### 2.1 High Dynamic Range (HDR) Technology

What makes HDR technology the latest evolution in digital media is that it captures, distributes, and displays the full range of luminance and color values that the human eye can perceive in real life [1]. Luminance is defined as the quantity of light arriving at the human eye and it is measured in  $\text{cd/m}^2$ . The human eye can adapt real world luminance and see a dynamic range of more than 14 orders of magnitude, which is the difference between highest and lowest luminance value in powers of ten [1]. However, at each single adaptation time, only a maximum of five orders of magnitude can be perceived by the human eye [1]. Fig. 2.1 illustrates the dynamic range of real world scenes and capabilities of the human eye, camera, and display.

HDR technology can cover the luminance range from  $0.005$  to  $10,000 \text{ cd/m}^2$ , close to what the human eye see. As opposed to HDR, SDR technology covers limited color gamut and dynamic range, ranging from  $0.1$  to  $100 \text{ cd/m}^2$ . As shown in Fig. 2.1, conventional SDR display can only show up to three orders of magnitude. HDR displays, however, can reach up to five orders of

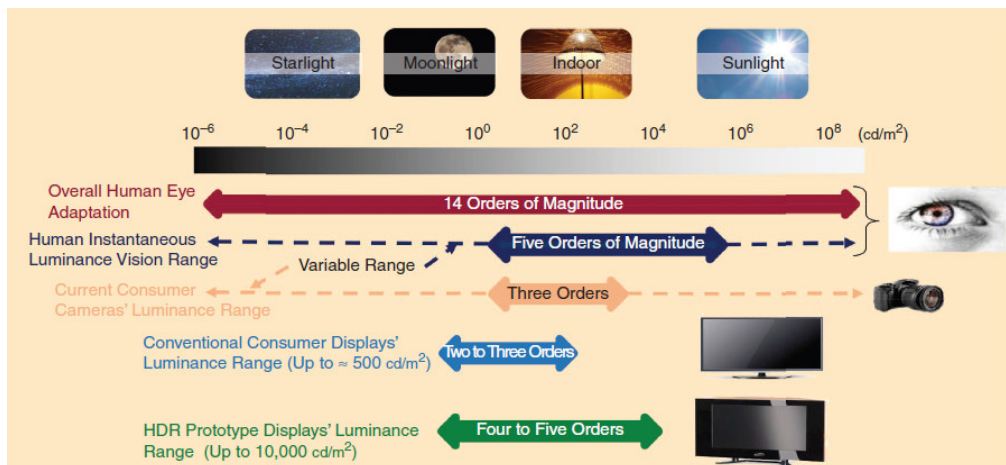


**Figure 2.1. The dynamic range of real world scenes and capabilities of the human eye, camera, and display [1]**

magnitude. When showing HDR and SDR contents with same scene on HDR and SDR displays respectively, viewers see more details and much more vivid colors on an HDR display, especially when the viewed sequences are under-exposed or over-exposed. Even when HDR content is tone-mapped in order to be seen on an SDR display, the resulting SDR content has way more details and is more pleasing to the human eye than the same content captured directly by an SDR camera [1] [13]. Fig. 2.2 shows a comparison between an SDR image and an HDR tone-mapped image of the same scene.



(a)



(b)

**Figure 2.2. Comparison between (a) an SDR image and (b) an HDR tone-mapped image**

## 2.2 Perceptual Encoding

When distributing HDR video, one challenge is the conversion from floating point light values to integer code values. This process, known as quantization, is necessary since existing video compression standards, such as the ITU-T H.265/High Efficiency Video Codec (HEVC) [14], only accept integer pixel values. In order to minimize the quantization error and preserve most of the pixel information, physical linear light intensities are perceptually transformed to a nonlinear domain. This transformation is known as perceptual encoding [15].

Perceptual encoding is useful for two reasons. The first one aligns with the fact that human eyes do not perceive light the same way cameras do [16]. Fig. 2.3 illustrates the camera and human eye's responses for incoming light. We observe that cameras capture light in a linear manner. Twice the luminance signal is received when luminance captured at the camera sensor is doubled (see red arrows in Fig. 2.3). However, human eyes are more sensitive to relative differences between dark tones than the same differences between bright tones, where twice the light is being perceived as

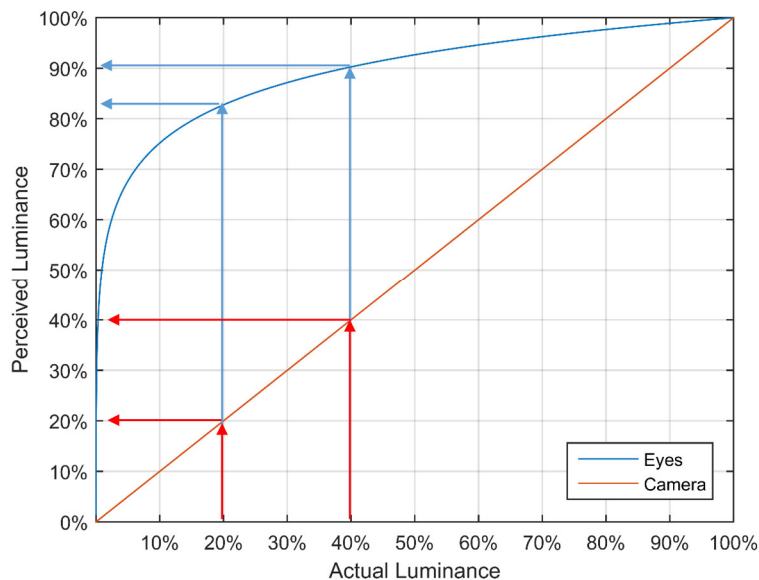


**Figure 2.3. Human eyes and cameras' responses for light**

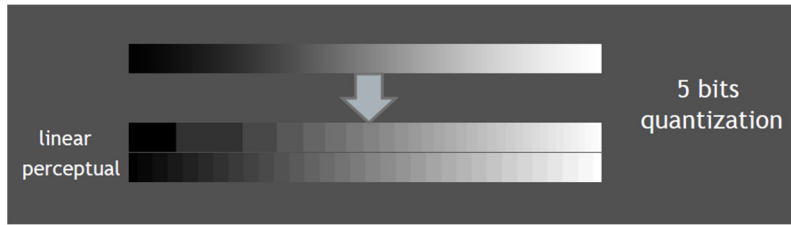


**Figure 2.4. Quantization for linearly encoded and perceptually encoded signals**

a fraction brighter for high light intensities (see blue arrows in Fig. 2.3). In fact, human eyes work in a nonlinear logarithmic relationship. Perceptual encoding simulates our eyes' response to light intensity (blue curve in Fig. 2.3). The second reason for applying perceptual encoding is to store brightness information more efficiently with fewer bits compared to linear encoding [16]. Using same bits for linearly encoded signal and perceptually encoded signal leads to more quantization errors (visible artifacts) for the former case (see Fig. 2.4). This is because, for linear signals, more bits are needed to describe the brighter tones where the human eyes are not very sensitive, while fewer bits are used for describing darker tones where we can really see the difference (see Fig. 2.4). Thus, with the close simulation of the human visual system (HVS), perceptually encoded signals need fewer bits to cover the whole tonal range during quantization.

Two commonly used perceptual encoding methods are gamma encoding [17], and perceptual quantization (PQ) [18]. Gamma encoding is designed for SDR content with luminance values up to 100 cd/m<sup>2</sup>. HDR displays, however, can reach up to luminance values of 10,000 cd/m<sup>2</sup>. For this reason, gamma encoding is not suitable for preparing HDR content. In order to efficiently encode HDR content and take advantage of the peak luminance of an HDR display, the Society of Motion Picture and Television Engineers (SMPTE) standardized the ST 2084 perceptual encoding, also known as PQ [19]. PQ is designed to handle HDR content with luminance ranging from 0.005 to 10,000 cd/m<sup>2</sup>. PQ projects light intensities to a more perceptually uniform domain. Visual

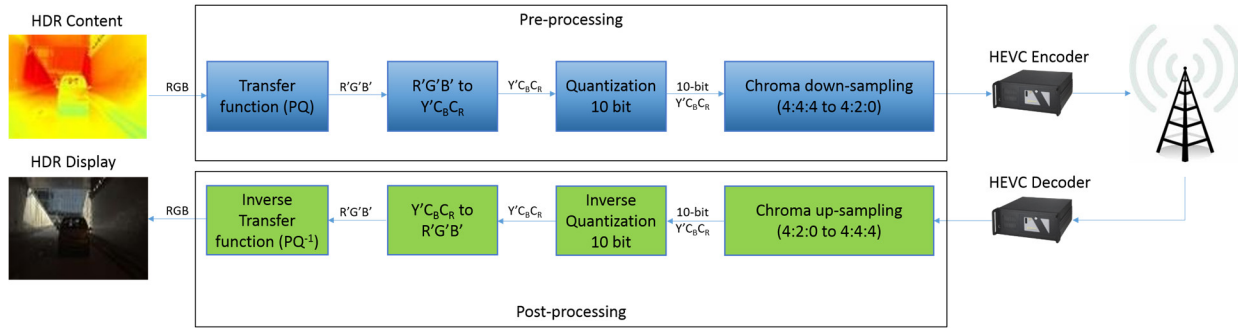


**Figure 2.5. General workflow of an HDR transmission pipeline**

degradation introduced by quantization is, therefore, spread out equally over the entire luminance range [4] (see Fig. 2.4). It is reported that only 11 bits are required for PQ to encode HDR signals without introducing any visual distortion [20].

### 2.3 High Dynamic Range (HDR) Transmission Pipeline

Once the HDR signal is quantized using PQ, as suggested by the Motion Picture Experts Group (MPEG), the HEVC Main 10 profile [21] can be used for compressing the signal. Fig. 2.5 shows the proposed workflows by MPEG for the transmission of HDR content based on HEVC Main 10 profile [21]. As it can be observed, RGB values first need to be converted into the luma and chroma format, known as Y'CbCr.

### 2.4 Color Encoding

To derive Y' from RGB values in the CL approach (represented as Yc' in this paper), perceptual encoding is applied to linear luminance (Y). Luminance signal is originally derived from a color matching experiment [9]. In this experiment, human observers are shown a target luminance light patch and another light patch next to it, which are generated by a weighted mixture of three color primaries (usually R, G, B) [22]. Subjects are asked to adjust the amount of each

primary so that the generated light patch visually matches with the target light. Eq. 1 shows how  $Y$  is derived:

$$Y = aR + bG + cB \quad (1)$$

where  $a, b, c$  are the weighting coefficients. This derivation is based on the fact that the human eye has three types of color sensors that respond to different ranges of the color spectrum [23]. Any color perceived by humans can be created by a linear combination of  $R, G,$  and  $B$ . In other words, color is three dimensional in the mathematical sense [24].

In the case of NCL,  $Y'$  is derived from perceptually encoded  $R'G'B'$  values using the CL weighting coefficients as follows:

$$Yn' = aR' + bG' + cB' \quad (2)$$

The workflows of the two encoding methods are shown in Fig. 2.6. Note that  $sf_{CB}$  and  $sf_{CR}$  are scaling factors for computing  $C_B$  and  $C_R$ .

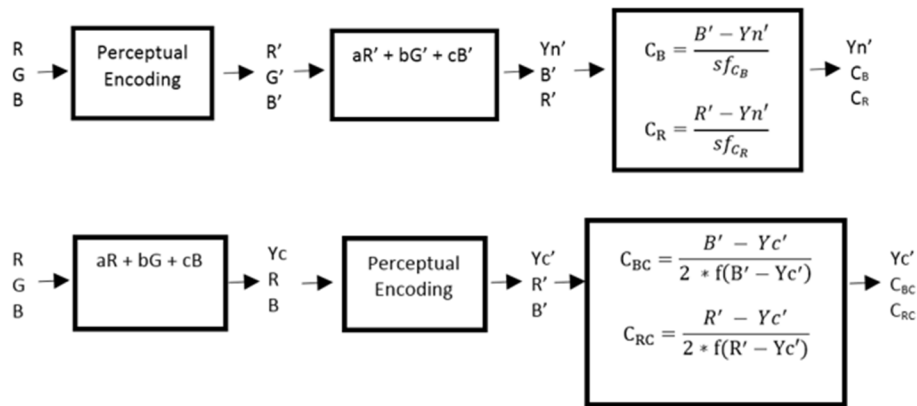


**Figure 2.6. Workflows of NCL (top), and CL (bottom) encoding methods**

The disadvantages of the conventional NCL representation include hue shift, less decorrelation of luma from the chroma signals, error propagation from chroma to luma information as described in [25], less resistance to chroma down-sampling, and lower compression efficiency as reported in [26]. Color shift is caused by applying PQ on R, G, and B channels individually. The highly non-linear PQ transfer function makes RGB values smaller, which in turn results in slightly darker pixels. The relative ratio between R, G, and B signals is also affected, thus resulting in a different shade of color. Since luminance is generated with a weighted linear combination of R, G, and B, color shift of RGB values leads to luminance errors between the original input and the resulted output luminance values.

Considering the above-mentioned problems related to the NCL method, the CL approach was introduced in the BT.2020 recommendation [5] to transmit physical luminance and offer improved coding efficiency. The CL approach results in higher color quality by better decorrelating light intensity from chromaticity. An in-depth analysis on NCL and CL methods presented in [26] reports less loss of original luminance information after chroma sub-sampling in the CL scheme. It was further proven that the CL approach has the benefit of higher compression efficiency over the traditional NCL method [26].

One main drawback of the CL method is the significantly increased implementation cost. For the CL case, the chroma values are dependent on a function of the difference between luma and  $B'/R'$  (see Fig. 2.6), which has to be calculated for each pixel. On the contrary, in the NCL case, only constants are needed for computing chroma signals as illustrated in Fig. 2.6. In the post-processing stage of the CL approach, recovery of the green signal needs help of inverse perceptual

encoding, which demands non-linear circuits [12]. Thus, the hardware implementation of CL approach dramatically diverts from that of the NCL method, offering no backward compatibility with legacy displays, which assume the input signal  $Y' C_B C_R$  is based on the NCL scheme. Because of the above and given that the vast installed base of content delivery pipelines are built around NCL, the broadcasting industry still prefers to follow the NCL encoding scheme [12]. Since cost and backward compatibility are prohibiting industry from adopting the CL approach, while HDR requires higher standards of compression efficiency and visual quality, optimizing the weighting coefficients for NCL perceptual encoded RGB values ( $R'G'B'$ ) seems to be an affordable alternative.

## 2.5 Luma Adjustment

As mentioned in the previous section, applying the conventional NCL approach results in color shifts and luminance errors between input and output luminance values. Luminance artifacts occur when the NCL method and a perceptual non-linear transfer function such as PQ are combined with 4:2:0 chroma sub-sampling [27]. This is because of the steep slope of PQ (see Fig. 2.7) in the low luminance range and the color transform from RGB to  $Y' C_B C_R$  [28]. Since NCL applies weighting coefficients on  $R'G'B'$ , which are perceptual encoded RGB values, individual color components (R, G, B) with low values, after PQ, have significant impact on  $Y'$ ,  $C_B$ ,  $C_R$  values. Pixels with similar colors, (0, 450, 470) and (1, 450, 470) for example (shown as RGB values), become dramatically different when converted to  $Y' C_B C_R$  space: (0.4907, 0.0952, -0.3328) and (0.5301, 0.0742, -0.2578). Then, 10-bit quantization, chroma down-sampling, chroma up-sampling, and 10-bit inverse quantization are applied as shown in Fig. 2.5. During decoding and just before displaying, the pixels are converted back to RGB values, which for the above example

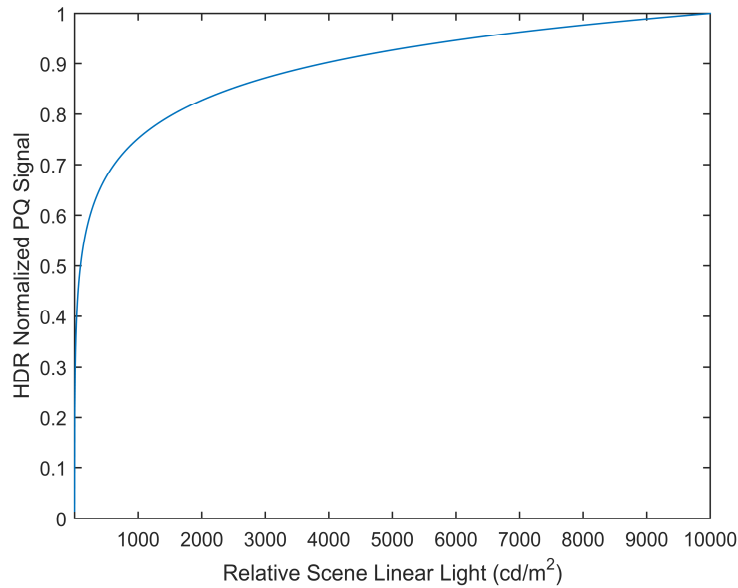


**Figure 2.7. PQ transfer function has steep slope at luminance values close to 0**

are (0, 431, 450) and (0, 617, 644), respectively. These two RGB outputs are significantly distorted colors comparing to the original ones. The steep slope of PQ combined with chroma down-sampling lead to color distortion for similar pixel values with one or two of the RGB components close to zero in the linear domain. These pixels have saturated colors located at the color gamut boundaries.

One method proposed in [27] to solve the above-mentioned problem of luminance errors is luma adjustment. This approach utilizes linear luminance, which is calculated the same way as that of CL method. luma adjustment solves them by up-sampling sub-sampled chroma components and then iterating over different luma values to choose the best luma signal that minimizes the difference between resulted linear luminance and that of the original RGB input [28]. Fig. 2.8 shows the workflow of luma adjustment.

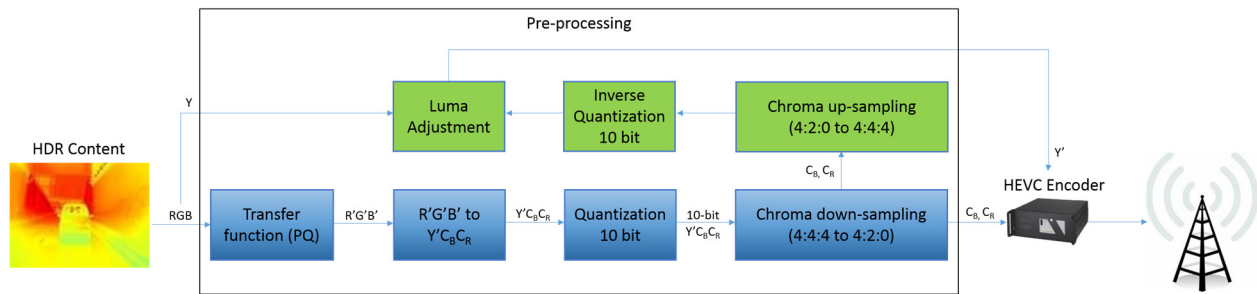


**Figure 2.8. Workflow of luma adjustment**

By taking advantage of “true” luminance, which corresponds to the physical luminance, luma adjustment shares the same idea as CL. However, luma adjustment requires several iterations, as high as ten, for calculating each luma sample for a 10-bit signal. Computation of the transfer function and color transformation at each iteration is time consuming, making the luma adjustment approach less practical [28].

### 3 Global Optimization of NCL to CL for HDR Video Distribution

#### 3.1 Introduction

Given the benefit of CL compression efficiency and its increased complexity, a natural solution is to seek reaching CL's efficiency with the NCL implementation. Since the CL coefficients  $a$ ,  $b$ , and  $c$  as described in BT.2020 [5] are designed for physical RGB values, they are not the best option for perceptually encoded  $R'$ ,  $G'$ , and  $B'$ . With this consideration in mind, we propose a global optimization method to derive new optimum coefficients that approximate NCL values to those of the CL approach.

#### 3.2 Proposed Method

In order to benefit from the CL compression efficiency without introducing its increased complexity, we propose to derive new coefficients  $d$ ,  $e$ ,  $f$  to globally minimize the difference between our generated alternative luma (denoted  $Y_{a'}$ ) and the CL luma  $Y_{c'}$ . Our optimization problem can, thus, be formulated as follows:

$$Y_{c'} = (aR + bG + cB)' \quad (3)$$

$$Y_{a'} = dR' + eG' + fB' \quad (4)$$

$$J = \operatorname{argmin} \|Y_{c'} - Y_{a'}\|^2 \quad (5)$$

$$= \operatorname{argmin} \sum_{k=1}^{2^{30}} (Y'_{ck} - Y'_{ak})^2$$

where newly derived coefficients  $d, e, f$  are between 0 and 1, and the sum of these three coefficients is constrained to be equal to 1. This optimization depends on the targeted bit-depth. In this thesis, we solely focused on 10 bits (around 1 billion R'G'B' code values, 30 bits per pixel).

Chroma scaling factors,  $sf_{CB}$  and  $sf_{CR}$ , as shown in the workflow of the NCL encoding method (see Fig. 2.5), are dependent on the maximum and minimum differences between B'/R' and Y'. The scaling factor,  $sf_{CB}$ , is calculated to ensure that  $C_B$  ranges from -0.5 to 0.5, as required in BT.2020 [5]. Eqs. (6) and (7) illustrate how  $sf_{CB}$  is derived in the NCL case. The same formula applies for  $sf_{CR}$ . Since a new different set of coefficients is generated ( $d, e, f$ ) that leads to a different luma ( $Y_{a'}$ ) value from that of the traditional NCL approach, new chroma scaling factors that depend on these new coefficients need to be computed. This can be easily accomplished by replacing  $Y_{n'}$  with  $Y_{a'}$  as shown below:

$$C_{B_{max}} = \frac{\max(B' - Y_{n'})}{sf_{CB}} = 0.5 \quad (6)$$

$$C_{B_{min}} = \frac{\min(B' - Y_{n'})}{sf_{CB}} = -0.5 \quad (7)$$

Solving the optimization problem from Eqs. (3) to (7) for a 10-bit R'G'B' input results in the following coefficients and scaling factors:  $d = 0.3365$ ,  $e = 0.4810$ ,  $f = 0.1825$ ,  $sf_{CB} = 1.6350$ , and  $sf_{CR} = 1.3270$ . Table 3.1 reports the average distortion between our computed luma ( $Y_{a'}$ ) and the CL luma ( $Y_{c'}$ ) over all R'G'B' combinations. The same table also reports the distortion between CL ( $Y_{c'}$ ) and the NCL luma ( $Y_{n'}$ ). We observe that our new coefficients provide a luma closer to that computed using the CL method when considering all R'G'B' combinations.

**Table 3.1: Comparison between our NCL ( $Y_{a'}$ ) and original NCL ( $Y_{n'}$ ) with CL ( $Y_{c'}$ ) over all possible 10-bit RGB combinations**

		Average Distortion
Our NCL	$\frac{1}{2^{30}} \sum_1^{2^{30}} \ Y_{c'} - Y_{a'}\ ^2$	0.0399
Original NCL	$\frac{1}{2^{30}} \sum_1^{2^{30}} \ Y_{c'} - Y_{n'}\ ^2$	0.0470

Note that our new coefficients need to be transmitted in order to reconstruct the R', G' and B' channels from  $Y_{a'}C_{B'}C_{R'}$  values. One way of achieving this, for example, is to send them via a Supplementary Enhancement Information (SEI) message [29] of the HEVC standard.

### 3.3 Results and Discussions

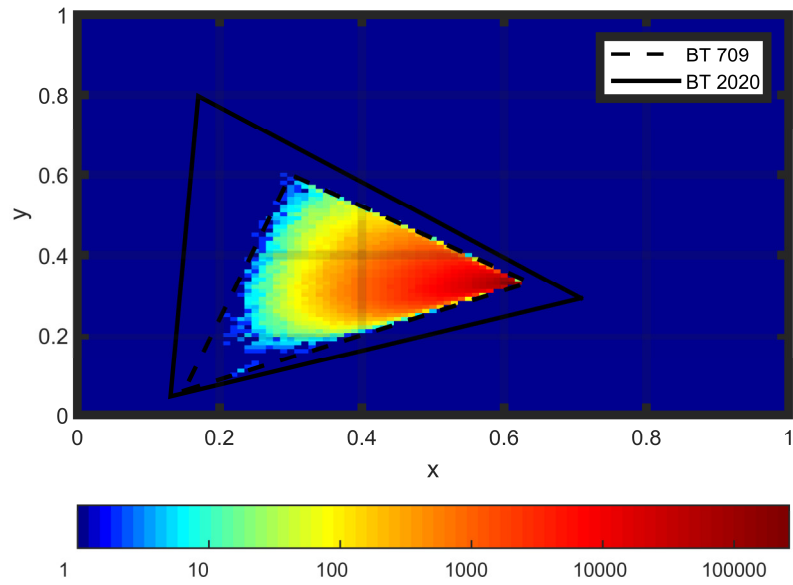
To compare the compression efficiency of our approach with the traditional NCL implementation, we encoded 5 HDR video sequences provided in the MPEG Call for Evidence (CfE) for HDR and WCG Video Coding [21]. Four different Quantization Parameters (QPs) were used with HEVC (version HM 16.7 [30]) according to MPEG recommendations. Two objective metrics; tOSNR-XYZ and DE100; were computed for each original and decoded frames, using the HDRTools software package v1.0 [31], and averaged over the whole sequence. The tOSNR-XYZ metric measures the overall PSNR for pixels in the XYZ color space. This metric measures the degradations of the signal when distributed throughout the pipeline. The DE100 metric is a PSNR computed using the CIEDE2000 [32] that predicts the color distortion between two pixels and includes perceptual aspect since it is based on the CIE L\*a\*b\* color space [33].

**Table 3.2: Average BD-rate reduction under the same visual and color quality**

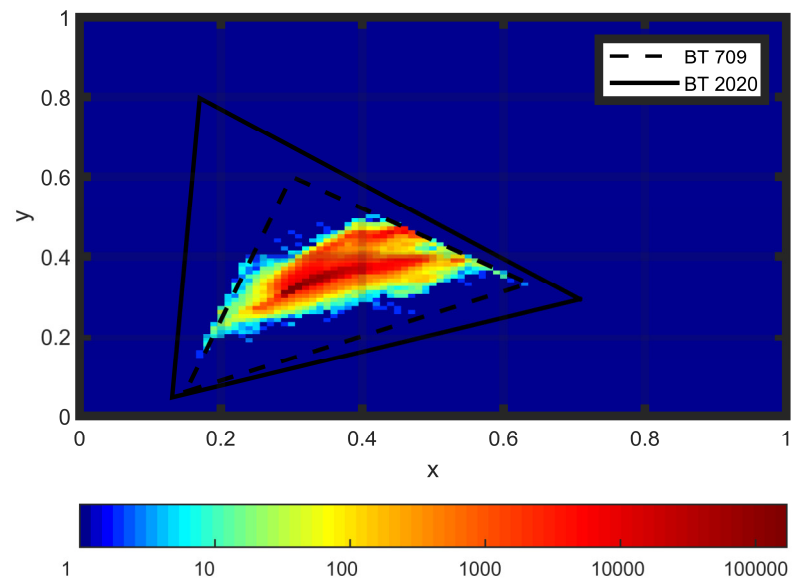
	tOSNR-XYZ	DE100
FireEater2	-7.8%	0.5%
Market3	-3.1%	33.0%
BalloonFestival	-5.7%	18.6%
Hurdles	-2.9%	24.2%
Start	-4.2%	26.7%
Average	-4.74%	20.6%

Table 3.2 reports the average bit-rate reduction (in percentage) for the same tOSNR-XYZ and DE100 values between our method and the NCL one. Bit-rate savings are measured using the Bjontegaard’s Delta (BD) Rate [34]. Negative numbers represent bit-rate reduction and positive numbers are equal to bit-rate increase. Thus, compared with NCL, our method always requires a lower bit-rate to achieve the same level of visual quality according to the tOSNR-XYZ metric. An average of 4.74% bit-rate reduction is achieved for keeping same overall visual quality. However, performance for color quality measured by DE100 is unsatisfactory, with an average of 20.6% bit-rate increase when maintaining the same level of color quality. In other words, compared with NCL, our method results in lower color quality when using the same bit-rate.

The reason behind the lower color quality is that our proposed global optimization treats all possible RGB values as equally important, which is not true for natural content. Figs. 3.1 and 3.2 show chromaticity distributions of two sample images (first frame of the content [35] [36]). Note that since the original content is BT.709 [6], all pixels fall within the BT.709 [6] color gamut boundary. In addition, we note that there are no pixels with dark blue while dark red represents more than 10,000 pixels. These two sample images have significantly different RGB distributions



**Figure 3.1. Chromaticity distribution for the first frame of the FireEater2 sequence in CIE 1931 color space**



**Figure 3.2. Chromaticity distribution for the first frame of the SunRise sequence in CIE 1931 color space**

and densities. Furthermore, these RGB inputs only occupy a fraction of all possible RGB combinations ( $2^{30}$  R'G'B' integer code values for 10 bits input). This indicates that natural contents have different RGB densities and each possible RGB combination has different weight (from 0 to a maximum of the resolution if all pixels have same RGB value). Thus, the resulted new coefficients have been compromised for RGB values (pixels) that do not exist in the video sequence.

### 3.4 Conclusion

We proposed a global optimization method to close the gap between NCL values and those of CL. A new set of coefficients for perceptually encoded R'G'B' values was derived to optimize NCL values. Focus was put on minimizing the difference between NCL luma ( $Y_n'$ ) and CL luma ( $Y_c'$ ).

We evaluated the performance of our method using two objective metrics recommended by MPEG for measuring HDR quality, tOSNR-XYZ and DE100. Results indicated that our proposed method has improved the visual quality according to the tOSNR-XYZ metric. An average of 4.74% bit-rate savings is observed for maintaining the same signal quality in the XYZ color space. For keeping the same color quality in the CIE L\*a\*b\* color space according to DE100, our method increases the bitrate by an average of 20.6%. This is because of the equal treatment of all possible RGB inputs by our approach. In reality, natural content has different RGB densities and distributions. Furthermore, these RGB values only occupy a fraction of all possible RGB inputs. Thus, our method optimizes too many pixels that are not included in the tested sequence.

We conclude that a better approach is to identify the existing color combination in a given HDR video stream and optimize the coefficients for the specific content. This leads to our next method.

## 4 Content Adaptive Optimization of NCL to CL for HDR Video Distribution

### 4.1 Introduction

For a 10-bit RGB input, the number of all possible RGB combinations is around 1 billion ( $2^{30}$  R'G'B' integer code values, 30 bits per pixel). Pixels from natural content contain only part of all possible RGB values. Thus, not all RGB combinations have equal importance.

As described in Section 3.3, when treating all RGB values as equally important with a global optimization method, the color quality is significantly reduced when keeping the same bit-rate as NCL. Since different HDR sequences have dramatically different RGB distributions, we propose a new adaptive optimization method for approximating NCL values to those of the CL approach, while preserving the NCL implementation. This new approach derives adaptive weighting coefficients based on the density of the pixels in a given HDR content.

### 4.2 Our Method

In the case of global optimization proposed in Chapter 3, each possible R'G'B' input has a weight of one. Since, as we already know, not all RGB combinations are included in natural content, coefficients have been compromised for optimizing pixels that may not exist in the video sequence. Based on this observation, we propose an adaptive optimization approach, which is based on the distribution of pixels for each content. This method perceptually encodes and quantizes all pixel values (RGB values) from the first frame of the chosen content into 10-bit integer code R'G'B' values. Then, the density of each R'G'B' combination is calculated by measuring the number of such integer code R'G'B' combinations. Note that for 10-bit input, the total number of all possible integer code R'G'B' combinations is  $2^{30}$ . Our method takes R'G'B'

density into consideration, and optimizes only the luma values of these R'G'B' inputs. Our optimization problem can, thus, be formulated as follows:

$$\begin{aligned}
 J &= \operatorname{argmin} W_k \|Yc' - Ya'\|^2 \quad (8) \\
 &= \operatorname{argmin} W_k \sum_{k=1}^{2^{30}} (Y'_{ck} - Y'_{ak})^2
 \end{aligned}$$

Note that newly derived coefficients  $d$ ,  $e$ ,  $f$ , as shown in Section 3.2 Eq. (4), are falling between 0 and 1. The sum of these three coefficients is constrained to be equal to 1, and the sum of all weights  $W_k$  ( $\sum_{k=1}^{2^{30}} W_k$ ) is equal to the resolution of the frame ( $1920 \times 1080 = 2073600$  in our case since all our video dataset is full HD). Note that no normalization is applied for  $W_k$ , since normalized  $W_k$  would be very small (i.e.,  $1/2073600$ ) and pixels with low  $W_k$  would be ignored in the optimization. Also note that new chroma scaling factors ( $sf_{CB}$  and  $sf_{CR}$ ) need to be re-calculated as they are dependent on the generated coefficients, as described in Section 3.2.

For a given HDR content, the first step is to identify all RGB pixel combinations within the first frame. The number of pixels with same RGB combination corresponds to the weight of that combination ( $W_k$ ), which is used in the optimization equation (8). Finally, the above-mentioned formulas (Eqs. 3, 4, 6, 7, and 8) are solved to get the new coefficients  $d$ ,  $e$ , and  $f$  for R'G'B' and the corresponding chroma scaling factors  $sf_{CB}$  and  $sf_{CR}$ .

Solving the optimization problem in Eq. (8) for different sequences results in different sets of coefficients. We chose eight HDR representative sequences in terms of brightness from the

**Table 4.1: New derived coefficients for contents**

	Coefficient (d)	Coefficient (e)	Coefficient (f)
FireEater2	0.3869	0.6131	0.0000
Market3	0.3299	0.5147	0.1554
SunRise	0.2778	0.6873	0.0349
Tibul2	0.4347	0.5653	0.0000
BalloonFestival	0.1956	0.7413	0.0631
Hurdles	0.3910	0.4730	0.1360
Start	0.3359	0.6324	0.0317
WalkPath	0.2459	0.7121	0.0420

video dataset provided in the MPEG CfE for HDR and WCG Video Coding [21]: Market3, FireEater2, Tibul2, SunRise [35], Hurdles, Start [37], BalloonFestival, and WalkPath [36]. Table 4.1 reports the new derived coefficients for all eight sequences.

### 4.3 Experiment Setup

To compare the compression efficiency of our method with the conventional NCL approach, we encoded eight HDR video sequences provided in the MPEG CfE for HDR and WCG Video Coding [21], as mentioned in the previous section. It is worth noting that although all these HDR contents are represented using the BT.2020 container, their values fall within the BT.709 color gamut. In our coding test, we used the latest HEVC codec software implementation (HM 16.7) with Main 10 profile [38]. For each HDR sequence, four different Quantization Parameters (QPs) were used as recommended by MPEG as shown in Table 4.2.

The objective metric DE100 was used to compute the color difference for each original and decoded frame, using the HDRTools software package v0.13 [38]; the results were averaged

**Table 4.2: Applied QPs for each content**

Sequence	Selected QPs
FireEater2	[20, 23, 26, 29]
Market3	[21, 28, 31, 33]
SunRise	[18, 21, 25, 29]
Tibul2	[19, 24, 29, 34]
BalloonFestival	[22, 26, 29, 31]
Hurdles	[23, 27, 32, 36]
Start	[22, 26, 32, 36]
WalkPath	[22, 26, 29, 31]

**Table 4.3: Average BD-rate reduction under the same color quality**

Sequence	DE100
FireEater2	-10.4%
Market3	27.5%
SunRise	-6.1%
Tibul2	-6.5%
BalloonFestival	-2.7%
Hurdles	22.7%
Start	-1.8%
WalkPath	-2.4%

over the entire sequence. As mentioned in the previous Chapter, the metric DE100 measures the color distortion between two pixels. We chose this metric according to MPEG recommendations and also the fact that it involves perceptual quality as well as color distortion.

## 4.4 Results and Discussions

Table 4.3 reports the average bit-rate reduction (in percentage) for the same color quality (same DE100 value) between our method and the NCL one. Bit-rate savings are measured via the Bjontegaard's Delta (BD) Rate [34]. Negative numbers represent bit-rate reduction while positive numbers are equivalent to bit-rate increase. Apart from sequences Market3 and Hurdles, lower bit-

rates are achieved for all other sequences compared with the traditional NCL scheme. These compression results suggest that for contents with extreme RGB distributions, Tibul2 and BalloonFestival (see Figs. 4.1, and 4.2), for example, improved color quality is possible due to the better weighted optimization and better decorrelation achieved by our method. Tibul2 has more red pixels while BalloonFestival has more deeply saturated green components as illustrated in Figs. 4.1, and 4.2.

Sequences with uniform chromaticity distributions, such as Market3 and Hurdles (see Figs. 4.3, and 4.4), however, do not benefit from our approach. This is due to the fact that these uniform distributed contents cover more chromaticity range than sequences with prominent red, green, or blue pixels. Thus, optimization for such content has similar effect to global optimization, which assigns the same importance to all possible RGB values. The new generated coefficients for

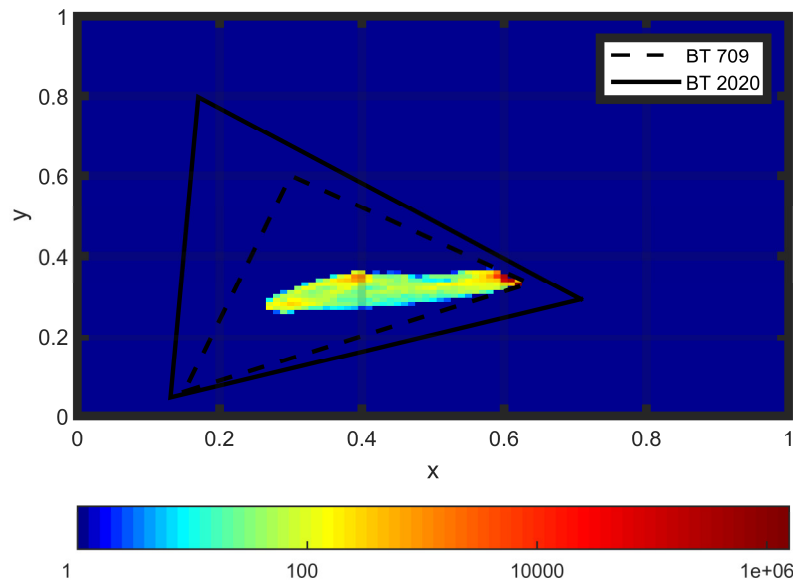


**Figure 4.1. Chromaticity distribution for the first frame of the Tibul2 sequence in CIE 1931 color space**

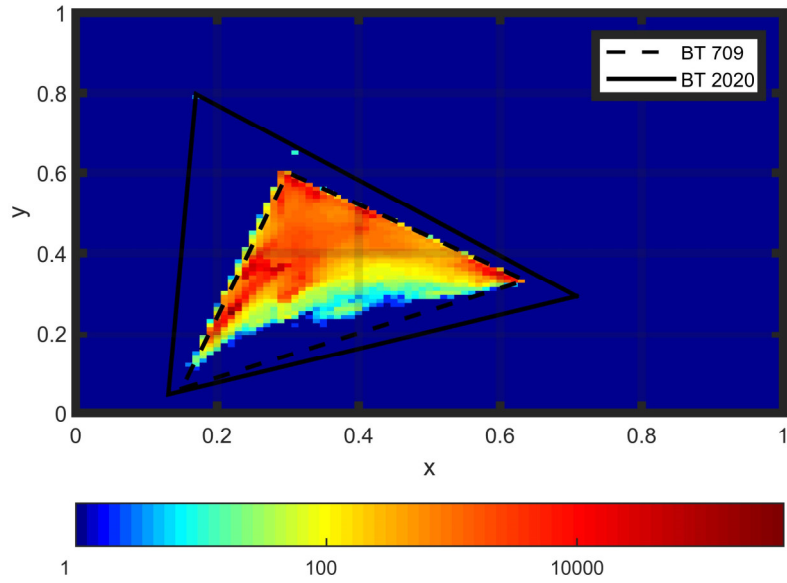


**Figure 4.2. Chromaticity distribution for the first frame of the BalloonFestival sequence in CIE 1931 color space**

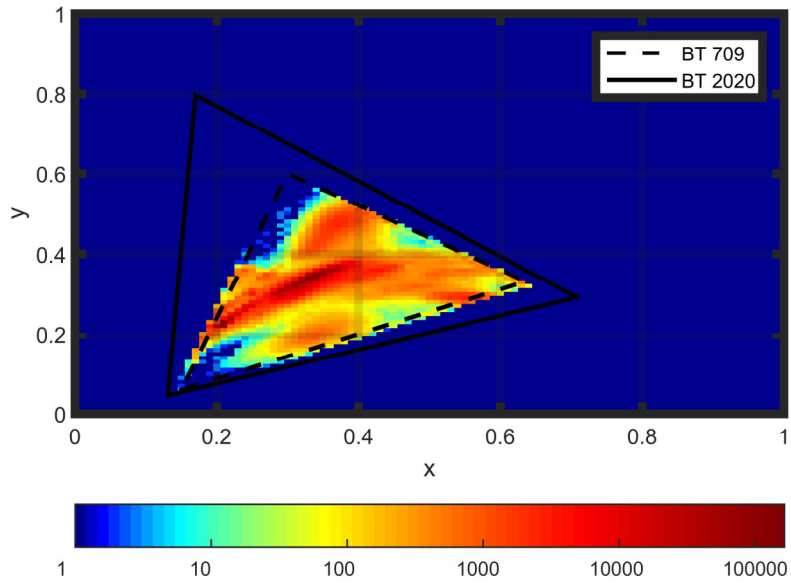


**Figure 4.3. Chromaticity distribution for the first frame of the Market3 sequence in CIE 1931 color space**

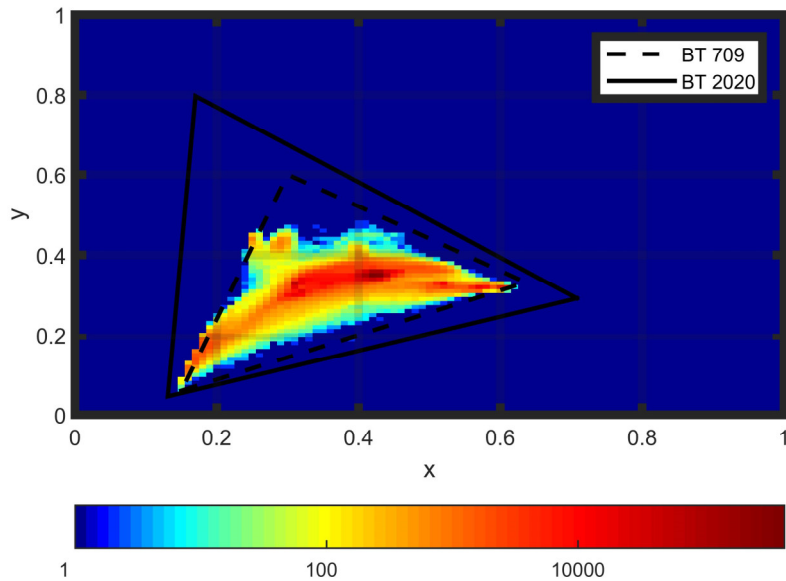


**Figure 4.4. Chromaticity distribution for the first frame of the Hurdles sequence in CIE 1931 color space**

Market3 and Hurdles share similar distributions and are pretty close to each other (see Table 4.1). As a matter of fact, these two sets of parameters are also close to the result of the global optimization method ( $d = 0.3365$ ,  $e = 0.4810$ ,  $f = 0.1825$ ). Unfortunately, treating all RGB inputs as equally important leads to reduced color accuracy compared with the NCL approach.

Figs. 4.5, 4.6, 4.7, and 4.8 plot the DE100 results for a dark HDR content (FireEater2), a normal daylight HDR content (BalloonFestival), and two broad daylight video sequences (Market3 and Hurdles). FireEater2 has red prominent signals and BalloonFestival is a green dominant sequence. Market3 and Hurdles are uniformly distributed video streams. We observe that our method yields higher DE100 values when considering the same bit-rates for FireEater2 and

BalloonFestival. The contrary is true for Market3 and Hurdels. These results are coherent with the percentages reported in Table 4.3.

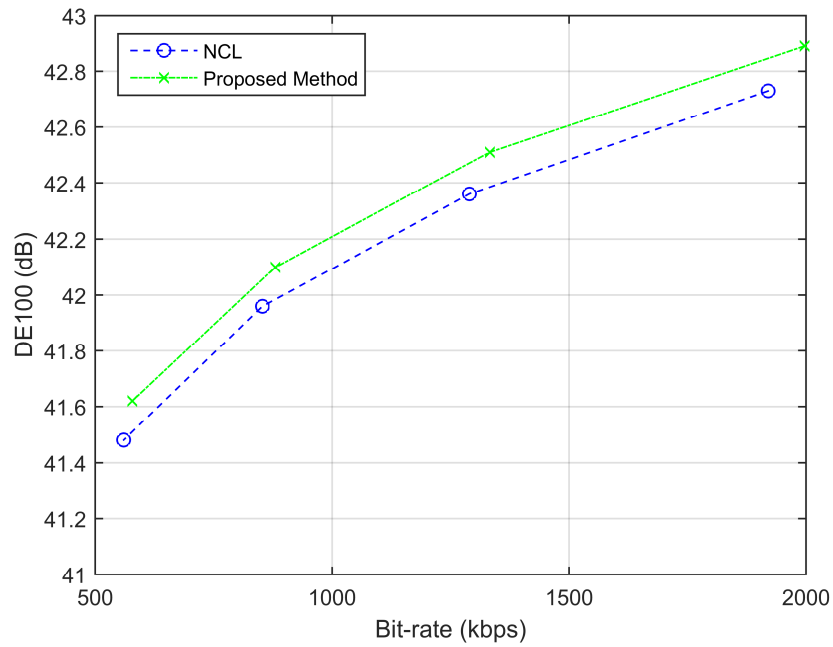


**Figure 4.5. DE100 vs bit-rate for FireEater2**

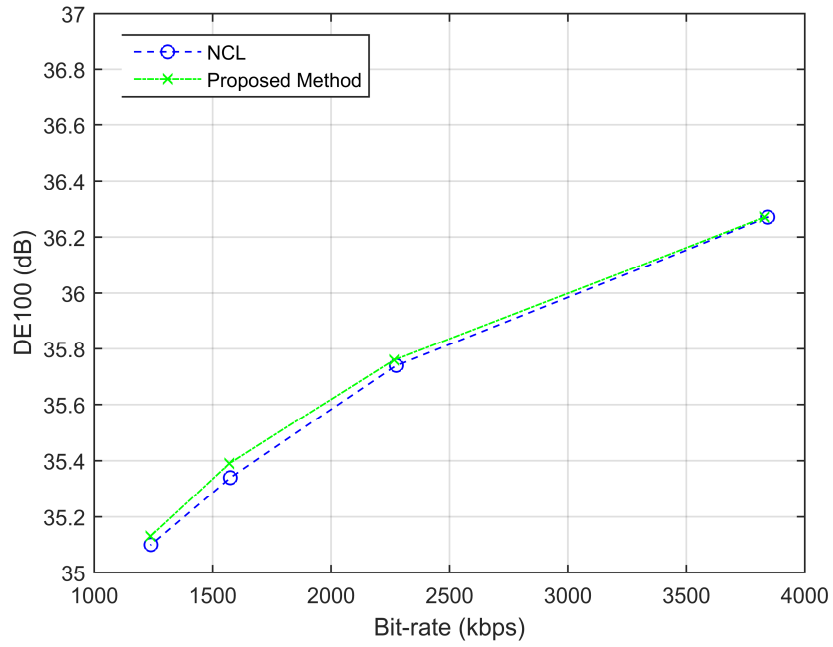


**Figure 4.6. DE100 vs bit-rate for BalloonFestival**

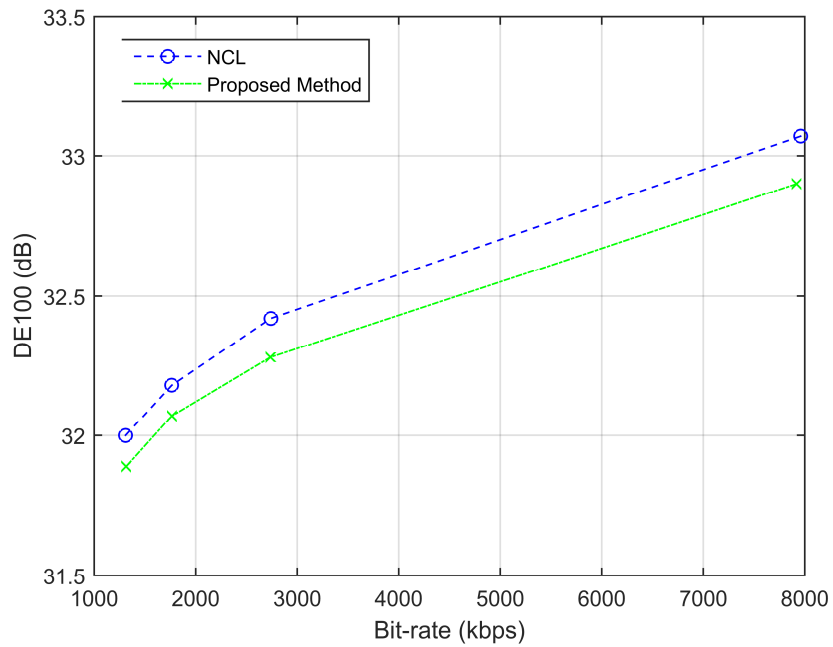


**Figure 4.7. DE100 vs bit-rate for Market3**

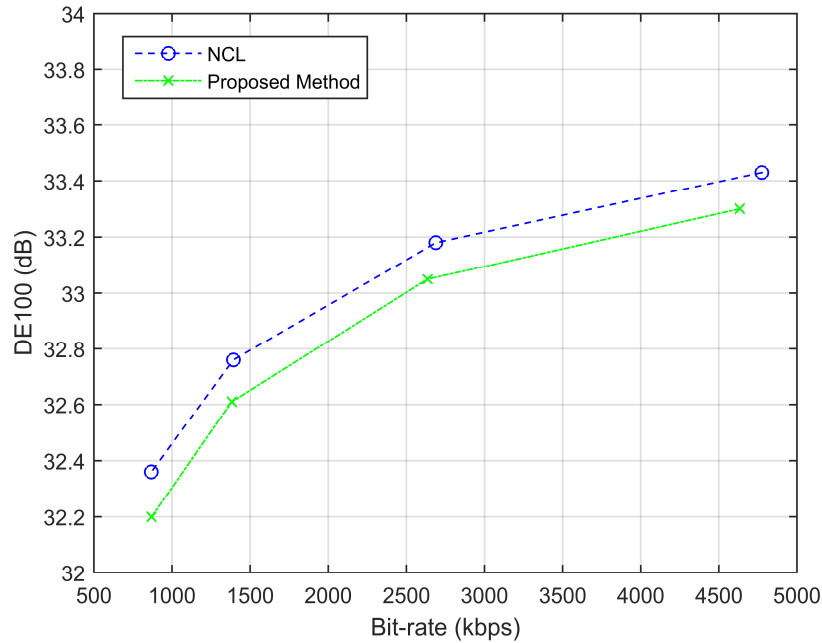


**Figure 4.8. DE100 vs bit-rate for Hurdles**

These results indicate that, based on the CIEDE2000 metric [32], our proposed method successfully increases the color quality over the NCL approach for content with extreme RGB distributions. For sequences with uniform chromaticity distributions, however, the NCL method can outperform our approach. Similar performance is expected for full range of BT.2020 [5] gamut content, when available. For uniformly distributed sequences, the former NCL coefficients can be sent with an SEI message. Note that the above-provided compression results do not include transmission of the new coefficients. However, transmission cost for these coefficients is negligible (as much as five 32 bits floating point values = 160 bits).

## 4.5 Conclusion

In this chapter, we proposed a content adaptive local optimization method that calculates new NCL coefficients based on the RGB pixel density for a specific HDR content.

Compression results showed that our proposed method yields improved color quality for content with one prominent primary (either R, G, or B). For such HDR sequences, an average of 4.98% bit-rate savings was observed for the same color quality according to the DE100 metric. However, for uniformly distributed sequences, our method did not offer better performance over the NCL approach. Given the fact that this method does not perform equally well for all video contents, we propose to use a hybrid approach, where we adaptively choose to either generate new coefficients and new chroma scaling factors using our proposed method or use the original NCL method, depending on the distribution of pixels in the specific HDR content.

## 5 Weighted Global Optimization of NCL to CL for HDR Video Distribution

### 5.1 Introduction

In Chapter 4, we proposed an adaptive optimization method to close the gap between NCL luma values and those of the CL. This approach takes RGB density of content into consideration and only optimizes based on these RGB values. As mentioned in Section 4.4, this proposed approach indicated that improved color quality can be achieved for extreme content cases where one of the RGB primaries (R, G, or B) is prominent. However, for HDR sequences with uniform chromaticity distributions, this method leads to reduced color quality compared with NCL. Since content with uniform chromaticity distribution covers more chromaticity range than a sequence with extreme red, green, or blue signals, adaptive optimization for such uniform distributed video has the same effect as the global optimization method mentioned previously. Thus, the generated coefficients for uniformly distributed content share similar distributions and are very close to the resulted coefficients from the global method.

In fact, in the global method the optimization error is spread out over all color values. However, according to the ITU-R Recommendation BT.2020 [5], the  $a$ ,  $b$ ,  $c$  coefficients for  $R'$ ,  $G'$ ,  $B'$  are:  $a = 0.2627$ ,  $b = 0.6780$ ,  $c = 0.0593$ . We observe that  $G'$  has the highest contribution to luma while  $B'$  is the least important one. The same trend can be observed in the ITU-R Recommendation BT.709 ( $a = 0.2126$ ,  $b = 0.7152$ ,  $c = 0.0722$ ) [6]. Since our objective is to minimize the luma difference between NCL and CL, we should put higher priority to greenish pixels and a lower priority to bluish ones during the optimization process for calculating the new  $a$ ,  $b$ ,  $c$  coefficients.

## 5.2 Our Proposed Method

Given the above-mentioned findings, we propose to derive new coefficients  $d$ ,  $e$ ,  $f$  that significantly reduce the difference between NCL and CL luma values by prioritizing the importance of RGB colors, with greenish being of the highest importance and bluish the lowest. In order to do this, we need to separate all possible colors into three important regions, Red, Green, or Blue. To categorize any pixel as either a Red, Green, or Blue dominant signal, we transform the RGB values into CIE  $xyY$  color space and map them on CIE 1931  $xy$  chromaticity diagram, which shows the full visible color gamut (see Fig. 5.1). Fig. 5.2 shows the full visible color spectrum and associated wavelength. Table 5.1 shows the actual wavelength ranges for the different colors. Fig. 5.3 presents an enhanced version of the CIE 1931  $xy$  chromaticity diagram (see [41] for more details).

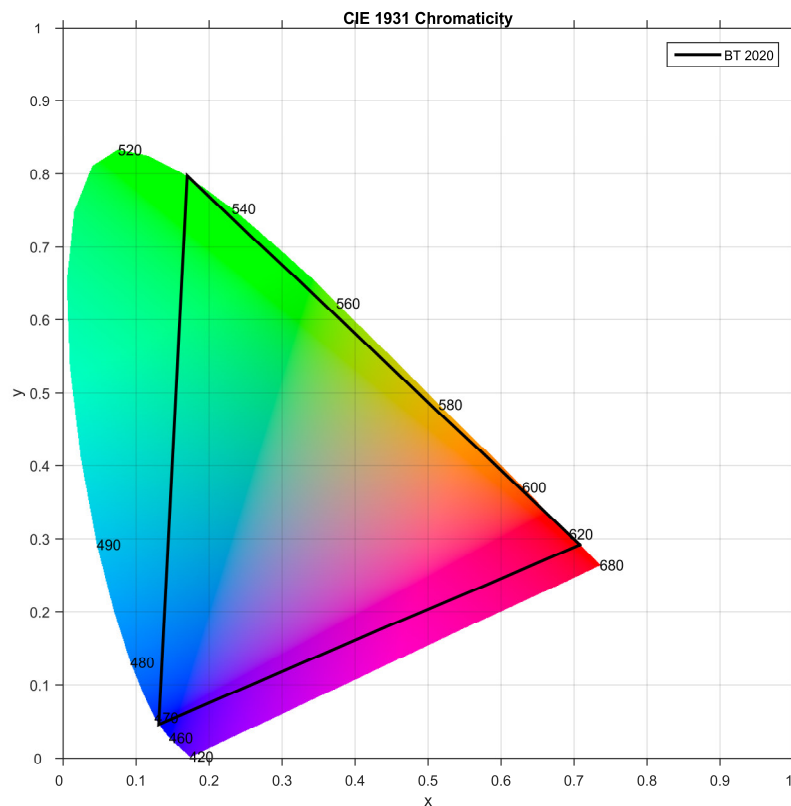


**Figure 5.1. CIE 1931  $xy$  chromaticity diagram with BT.2020 gamut coverage**

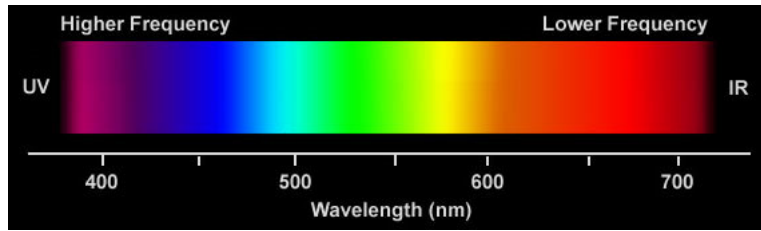


**Figure 5.2. The full visible color spectrum and associated wavelength [39]**

**Table 5.1: Visible color wavelength range [40]**

Color	Wavelength (nm)
Violet	380 - 450
Blue	450 - 495
Green	495 - 570
Yellow	570 - 590
Orange	590 - 620
Red	620 - 750

Separation between Blue and Green is approximately 500 nanometers (nm) according to Table 5.1. Yellow pixels are closer to green as shown in the chromaticity diagram (see Fig. 5.3). Yellow RGB pixel, (255, 255, 51), for example, is more greenish since G has more contributions to luminance than R (when G, and R components have same value). Orange, as illustrated in Fig. 5.3, is closer to red and is, therefore, more reddish. An orange RGB pixel, (255, 128, 0), for instance, has higher R component than that of G. Thus, we put yellow pixels into the Green category, and orange pixels into the Red category. Separation between yellow and orange is roughly 600 nm as described in both Fig. 5.3 and Table 5.1.

The remaining question is how to separate the Blue and Red sections. Since violet is closer to red as seen in Figs. 5.1 and 5.3, we drew the line to point to (0.3, 0) on the x axis of the CIE

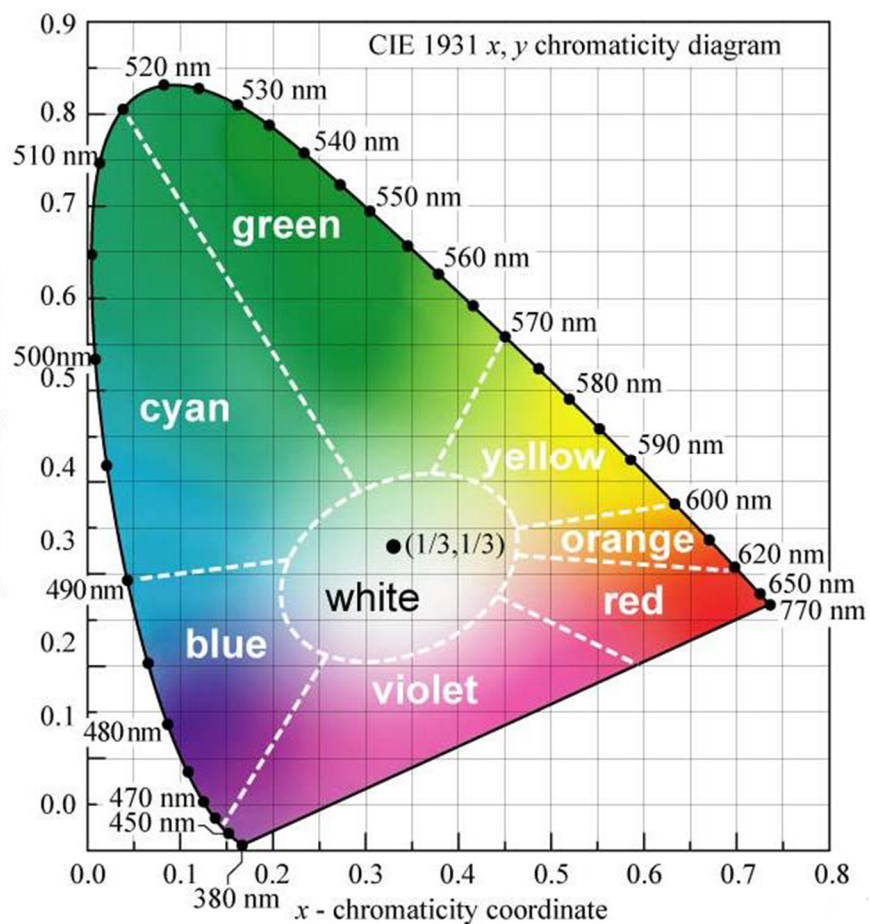


**Figure 5.3. Enhanced CIE 1931 xy chromaticity diagram with divisions for different colors [41]**

1931 xy chromaticity diagram. This ensures that more than 50 percent of the violet pixels belong to the Red category. Based on the above observations, we classify the colors into a Red dominant region, a Blue dominant region and a Green dominant region as shown in Fig. 5.4.

Once all the RGB samples in the BT.2020 gamut are separated into three regions of Red, Green, and Blue, we assign different priority to the optimization error corresponds to each RGB sample based on its region in the BT.2020 gamut and calculate new coefficients d, e, and f as follows:

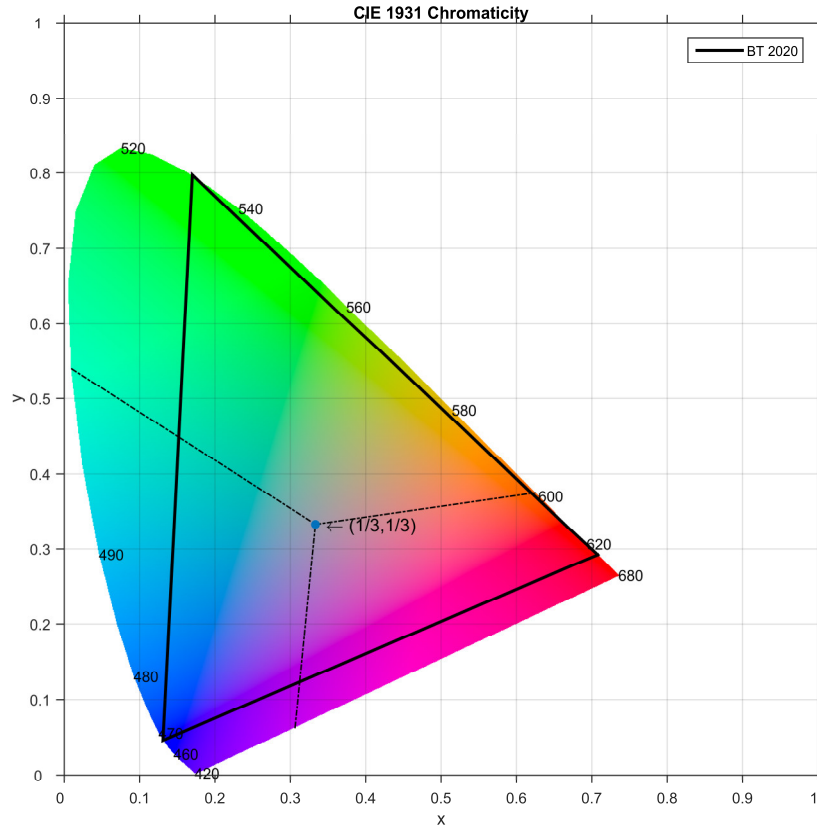


**Figure 5.4. Separation of CIE 1931 xy chromaticity diagram into Red, Green, and Blue**

$$J = \operatorname{argmin} W_k \|Yc' - Ya'\|^2 \quad (9)$$

$$= \operatorname{argmin} W_k \sum_{k=1}^{2^{30}} (Y'_{ck} - Y'_{ak})^2$$

where coefficients  $d, e, f$  are the newly derived coefficients that are summed to 1, and  $W_k$  is the weight for each RGB sample. The weights ( $W_k$ ) for samples are calculated based on the distribution of coefficients  $a, b$ , and  $c$  from BT.2020 [5]. In other words if the RGB sample falls into the Red region the weighting factor ( $W_k$ ) is equal to  $a$ , if it is in the Green region  $W_k$  is equal to  $b$ , and if it is in the Blue region it is equal to  $c$ . To avoid normalization and ensure that these weights are not being ignored during optimization, we multiply  $a, b, c$  by 100. Since PQ covers the luminance

range from 0.005 to 10,000 cd/m<sup>2</sup>, the lowest luminance value for non-zero RGB samples (at least one of the RGB channels is larger than 0) should be 0.005 cd/m<sup>2</sup> when deriving new coefficients. Note that all RGB inputs that have luminance value below 0.005 will be clipped to 0.005 during perceptual encoding. Thus, the lowest luminance value for linear RGB is 0.005 and the corresponding lowest luma value for perceptually encoded RGB (R'G'B') is 0.0151. To satisfy this condition, coefficients  $d$ ,  $e$ ,  $f$  need to be constrained to range from 0.0151 to 1. Again, note that the above optimization depends on the used color gamut primaries and targeted bit-depth. In this thesis, we focused on BT.2020 color gamut and 10 bits ( $2^{30}$  R'G'B' code values, 30 bits per pixel). Also note that new chroma scaling factors,  $sf_{CB}$  and  $sf_{CR}$ , dependent on new coefficients should be calculated.

Solving the above-mentioned optimization problem (Eqs. 3, 4, 6, 7 and 9) for a 10-bit R'G'B' input results in the following coefficients:  $d = 0.2590$ ,  $e = 0.7259$ ,  $f = 0.0151$ ,  $sf_{CB} = 1.9698$ , and  $sf_{CR} = 1.4820$ . Once more, please note that our new coefficients need to be transmitted in order to reconstruct R'G'B' from  $Ya'C_B C_R$  values at the decoding stage. One way of achieving this, for instance, is to send them via an SEI message of HEVC.

### 5.3 Experiment Setup

To compare the compression efficiency of our approach with the traditional NCL method, we encoded 8 representative HDR video sequences provided in the MPEG CfE for HDR and WCG Video Coding [21]: Market3, FireEater2, Tibul2, SunRise [35], Hurdles, Start [37], BalloonFestival, and WalkPath [36]. All these HDR contents fall within the BT.709 gamut [6].

But their values are represented using the BT.2020 [5] container. Table 5.2 summarizes the characteristics of each sequence.

**Table 5.2: HDR video dataset**

Sequence	Frame rate (fps)	Number of frames	Bit depth	Scene type
FireEater2	25	200	10	Outdoor/ Night light
Market3	50	400	10	Outdoor/ Day light
SunRise	25	200	10	Outdoor/ Day light
Tibul2	30	240	10	Outdoor/ Day light
BalloonFestival	24	240	10	Outdoor/ Day light
Hurdles	50	500	10	Outdoor/ Day light
Start	50	500	10	Outdoor/ Day light
WalkPath	24	240	10	Outdoor/ Day light

**Table 5.3: Applied QPs for each content**

Sequence	Selected QPs
FireEater2	[20, 23, 26, 29]
Market3	[21, 28, 31, 33]
SunRise	[18, 21, 25, 29]
Tibul2	[19, 24, 29, 34]
BalloonFestival	[22, 26, 29, 31]
Hurdles	[23, 27, 32, 36]
Start	[22, 26, 32, 36]
WalkPath	[22, 26, 29, 31]

In our test, we used the HEVC codec, Main 10 profile (test model software HM 16.7 [30]). HEVC is the most recent video compression standard [42], which has 50% more compression efficiency over its predecessor H.264/Advanced Video Coding (AVC) [43]. Four different Quantization Parameters (QPs) were used with according to MPEG recommendations. Table 5.3 shows the QP values used for each content. Note that the 10-bit quantization performed throughout the study follows the restricted range quantization as described in the ITU-R Recommendation BT.2100 [44].

Two objective metrics tOSNR-XYZ and DE100 were computed for each original and decoded frame, using the HDRTools software package v0.13 [38], and the results were averaged over the whole sequence. The tOSNR-XYZ metric measures the overall PSNR for pixels in the XYZ color space. It also measures the degradations of the signal when transmitted through the pipeline. The DE100 metric is a PSNR quantified version of the CIEDE2000 metric [32], which predicts the color distortion between two pixels [33].

## 5.4 Results and Discussions

Table 5.4 reports the average bit-rate reduction in percentage for the same DE100 value between our method and the NCL one (column 3). Bit-rate savings are measured using the Bjontegaard’s Delta (BD) Rate [34]. Negative numbers represent bit-rate reduction and positive numbers indicate bit-rate increase. We observe that, the same level of color quality according to the DE100 metric, our method results in 4.9% bit-rate reduction on average. These results suggest that improvement in color quality is possible due to the better weighted global optimization and better decorrelation of luma from chroma achieved by our method.

The results for tOSNR-XYZ metric are also reported in Table 5.4 (column 2). We observe that, for the same overall visual quality measured by tOSNR-XYZ, our method requires a minimal 2.23% increase in bitrate compared to the NCL approach.

**Table 5.4: Average BD-rate reduction under same visual and color quality**

Sequence	tOSNR-XYZ	DE100
FireEater2	2.5%	-1.1%
Market3	1.6%	-5.6%
SunRise	2.5%	-14.1%
Tibul2	1.6%	-1.0%
BalloonFestival	2.4%	-6.2%
Hurdles	1.7%	-4.7%
Start	2.7%	-2.5%
WalkPath	2.8%	-4.0%
Average	2.23%	-4.9%

Figs. 5.5, 5.6, 5.7 and 5.8 plots the tOSNR-XYZ compression results for a dark light HDR content (FireEater2), two broad daylight video sequences (Market3 and Hurdles), and a normal daylight sequence (SunRise). We observe that, on each plot, the two curves are nearly identical. This observation translates to same tOSNR-XYZ performance for both techniques, at any chosen QP, and the bit-rates are slightly different. This result is consistent with the numbers reported in Table 5.4. Figs. 5.9 to 5.12 describe the DE100 results for same four sequences. Our method always has higher DE100 values when considering the same bit-rates for all contents. Once more, these results follow those reported in Table 5.4.

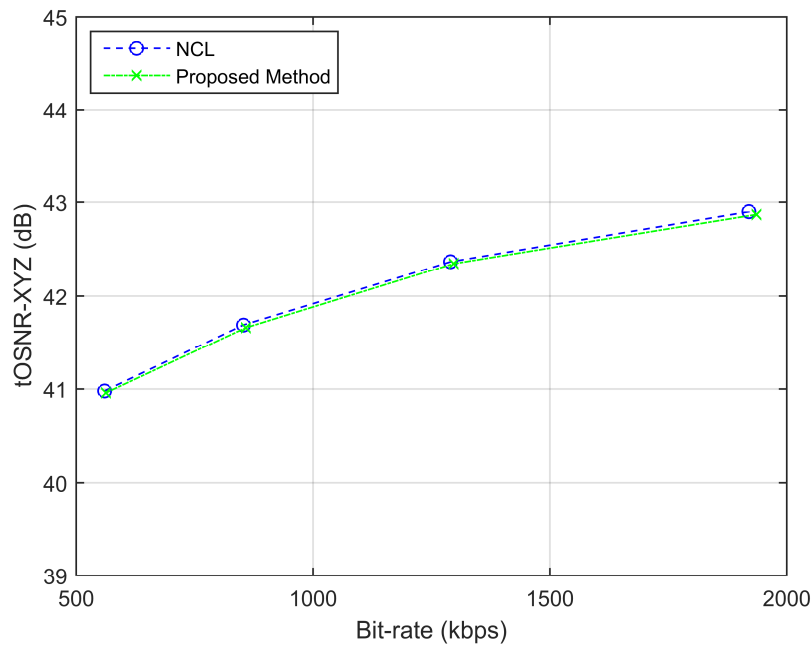


**Figure 5.5. tOSNR-XYZ vs bit-rate for FireEater2**

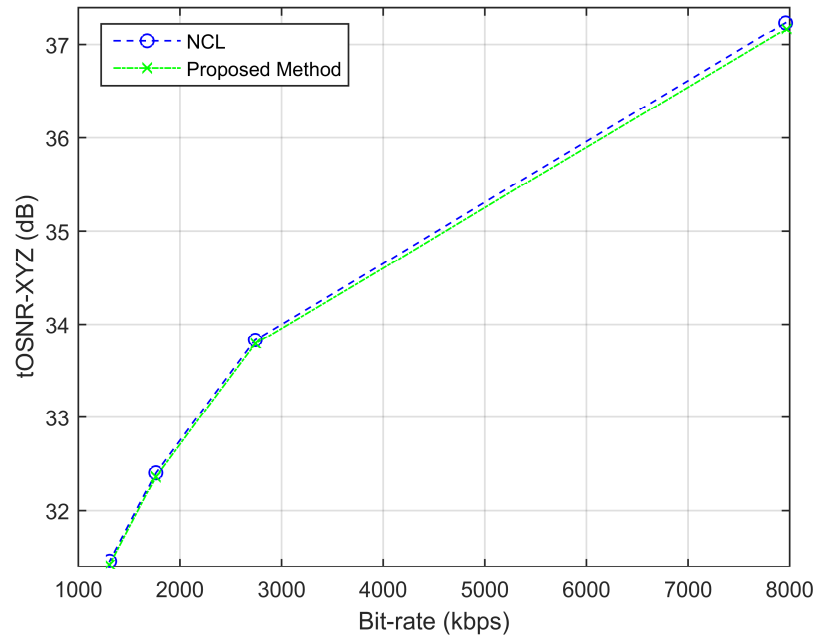


**Figure 5.6. tOSNR-XYZ vs bit-rate for Market3**

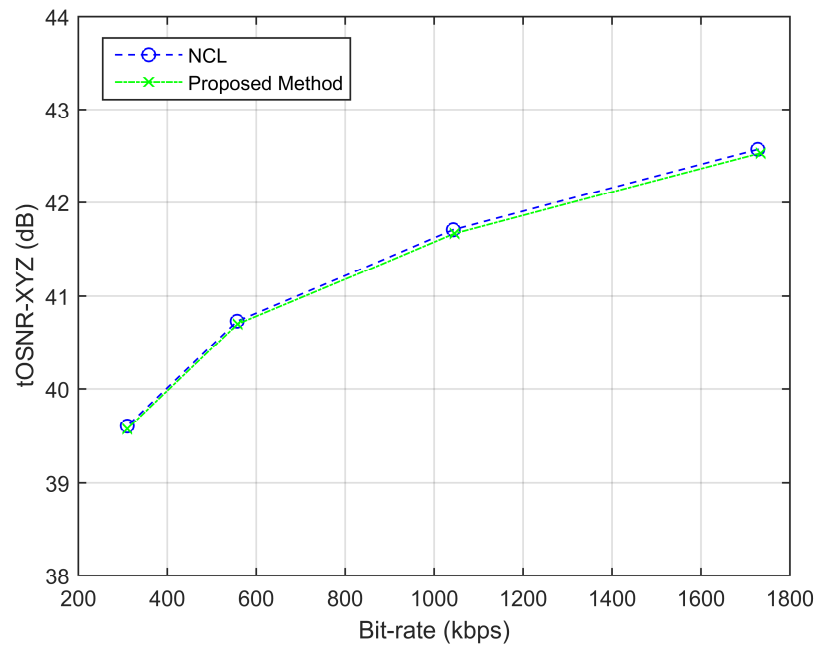


**Figure 5.7. tOSNR-XYZ vs bit-rate for SunRise**

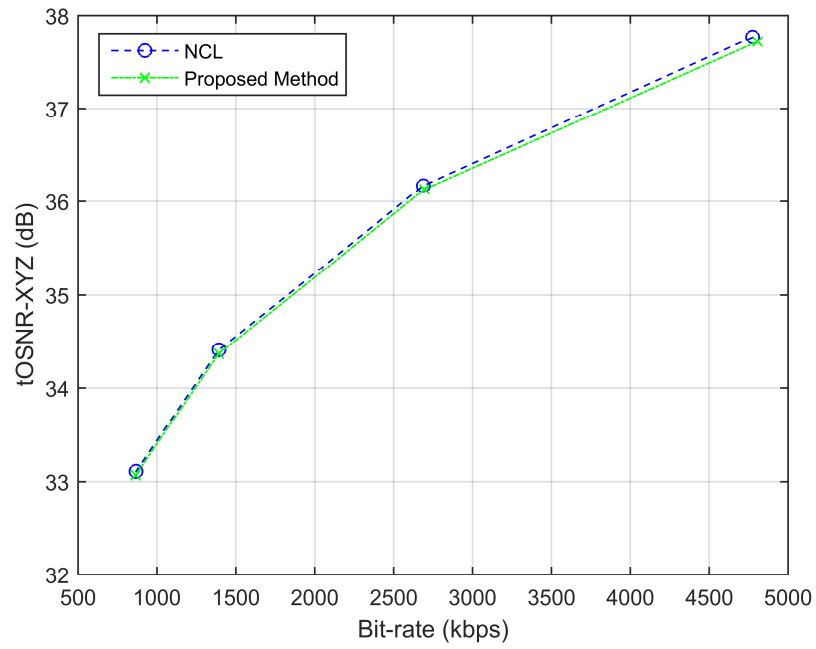


**Figure 5.8. tOSNR-XYZ vs bit-rate for Hurdles**

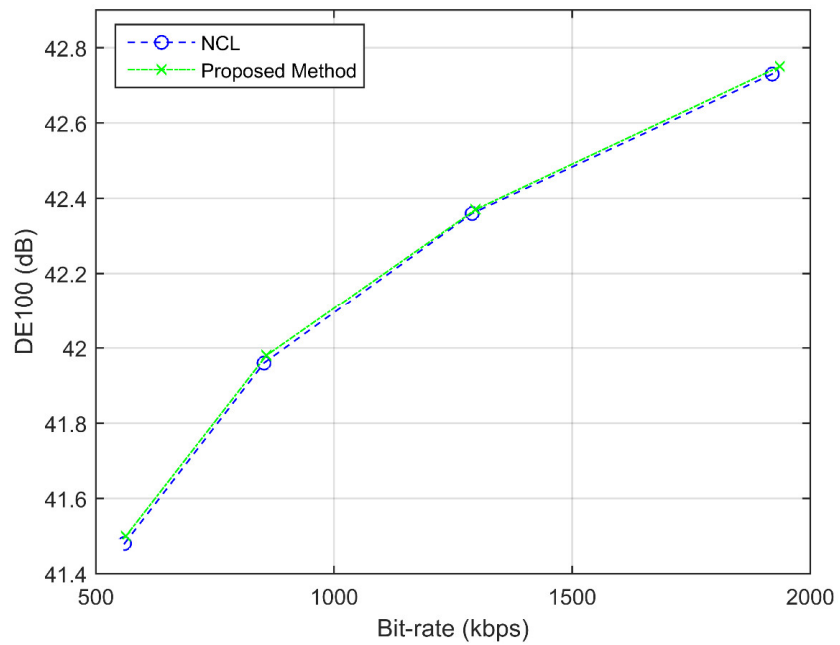


**Figure 5.9. De100 vs bit-rate for FireEater2**

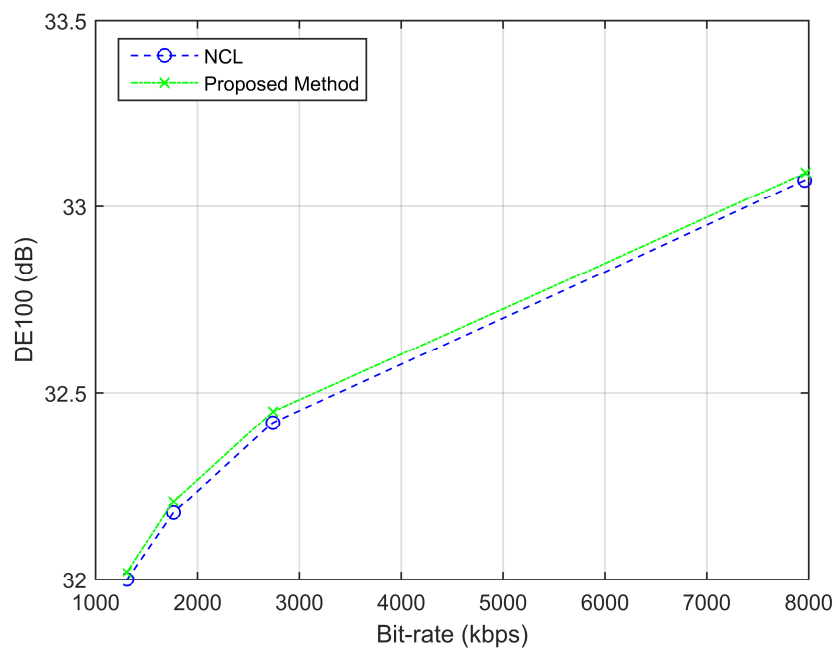


**Figure 5.10. DE100 vs bit-rate for Market3**

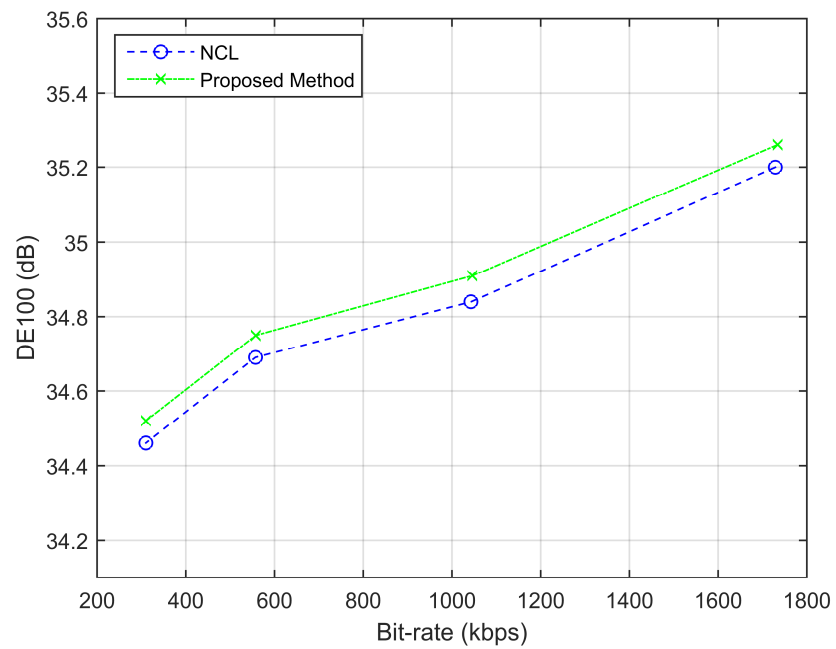


**Figure 5.11. De100 vs bit-rate for SunRise**

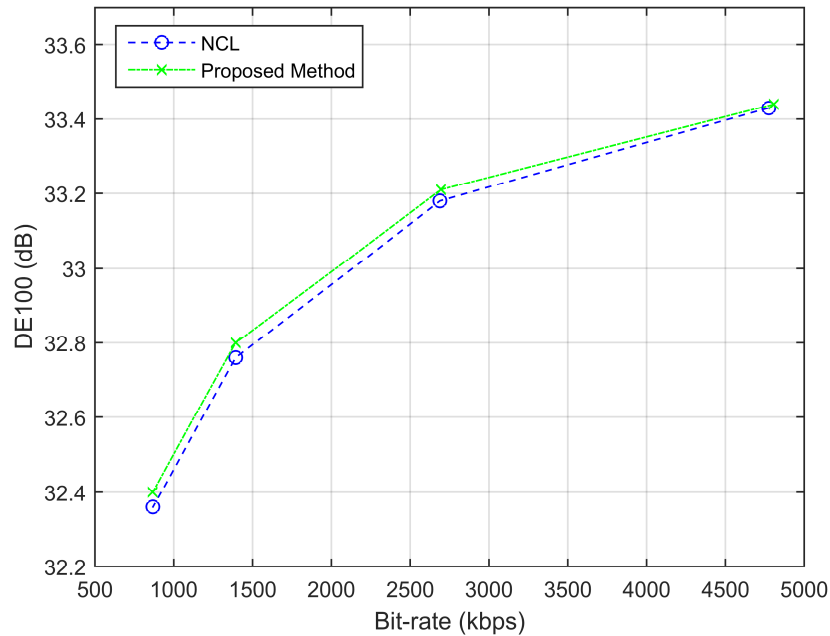


**Figure 5.12. DE100 vs bit-rate for Hurdles**

Since the chosen HDR sequences are limited and may not be representative of all the scenes we see in the real world, we also measured the visual color difference of all possible colors between our method and the NCL one. We evaluated the color distortion for 10-bit quantization without compression by encompassing all the visible colors of the BT.2020 [5] color gamut at different luminance levels. A perceptual color error metric, CIEDE2000 [32], as mentioned in the previous section, is used to predict visual color difference. In order to isolate the quantization errors, no chroma sub-sampling is applied. Fig. 5.13 shows the workflow of our evaluation process. Note

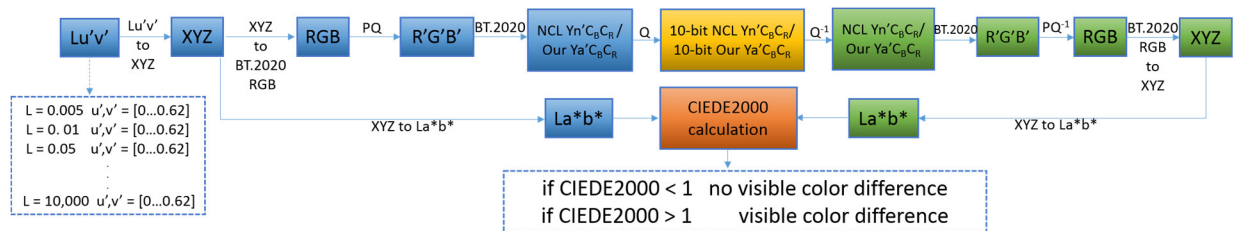


**Figure 5.13. Color difference experiment workflow**

that the 10-bit quantization performed here again follows BT.2100 [44]. To measure the color deviations of the tested signal (green boxes in Fig. 5.13) from the original signal (blue boxes in Fig. 5.13), we applied the perceptual objective metric CIEDE2000 [32]. Since this metric is designed to work on CIE L\*a\*b\* color space [33], the original and the recovered signals are transformed to this color space for comparison (see Fig. 5.13). The Just Noticeable Difference (JND) threshold of CIEDE2000 is one [45], which means color difference lower than 1 is not perceptible by the human eye [46]. Furthermore, the larger the CIEDE2000 value, the more different the tested color are perceptually [46].

Our test includes all visible colors within BT.2020 [5] gamut and for luminance levels ranging from 0.005 to 10,000 cd/m<sup>2</sup>. We chose the CIE 1976 Lu'v' color space [47] to construct these colors due to its perceptual uniformity [48]. At each luminance level, the u' and v' values are increased from 0 to 0.62 with a step size of 0.001, while L is kept constant. The threshold of 0.001 is chosen because chromaticity changes lower than this value are not perceptible to the human eye according to [49].

Figs. 5.14, to 5.21 illustrate the color distortion generated by the 10-bit NCL method and our proposed 10-bit color encoding scheme at each luminance level. The different luminance levels selected are: 0.005, 0.01, 0.05, 0.1, 1, 5, 10, 50, 100, 250, 500, 1000, 5000, and 10,000 cd/m<sup>2</sup>. We used a color error bar to demonstrate the CIEDE2000 values. Dark blue represents values below the JND (less than 1) and dark red corresponds to values more than or equal to 3. Thus, color distortion becomes visible when light blue starts to appear. Note that shortage of colors (less coverage of BT.2020 gamut) at luminance level of 0.005, 0.01, 1,000, 5,000 and 10,000 cd/m<sup>2</sup> is

due to the clipping forced by generated luminance levels above the specified range. It can be observed that color errors occur mainly around the white point [50] [51]. This happens because human eyes are more sensitive to luminance change than chrominance change. Since colors near the white point are much brighter (see Fig. 5.3), errors caused by quantization are more visible and, thus, result in higher CIEDE2000 values.

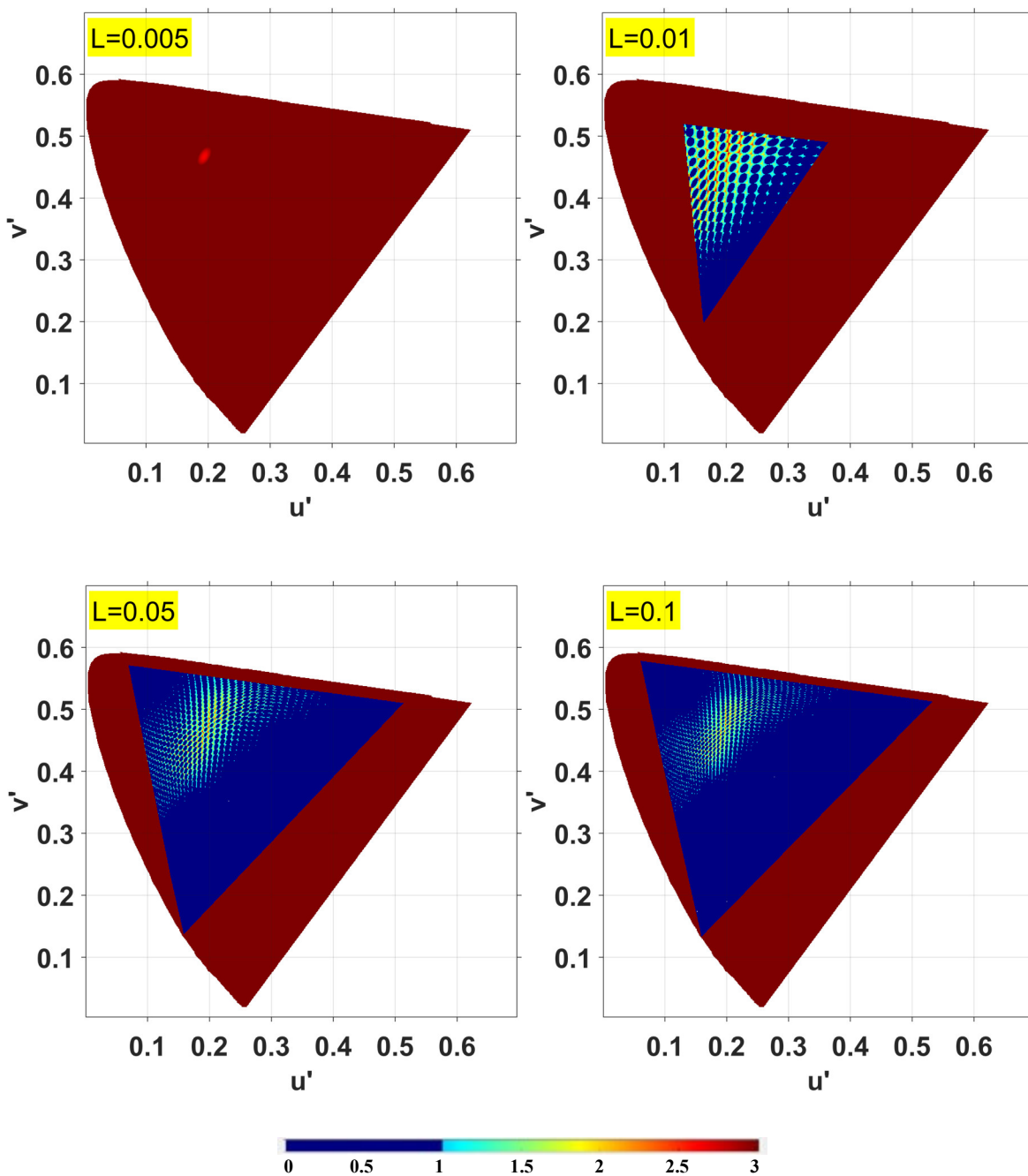


**Figure 5.14. Color distortion at different luminance levels (0.005 to 0.1  $\text{cd}/\text{m}^2$ ) for 10-bit NCL  $Y_n'$ CBCR with PQ transfer function**

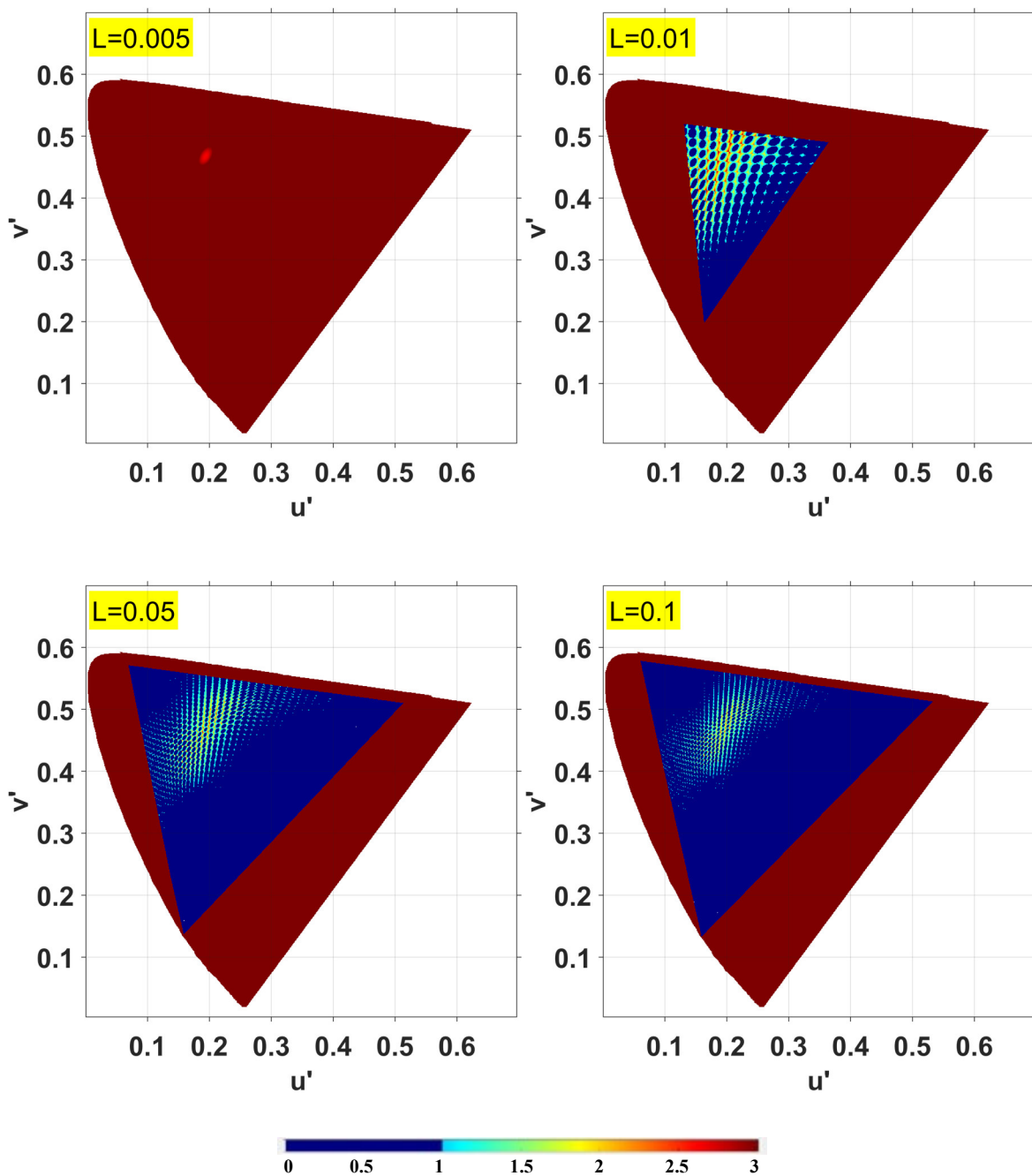


**Figure 5.15. Color distortion at different luminance levels (0.005 to 0.1  $\text{cd}/\text{m}^2$ ) for 10-bit our proposed  $Y_a'$ CBCR with PQ transfer function**

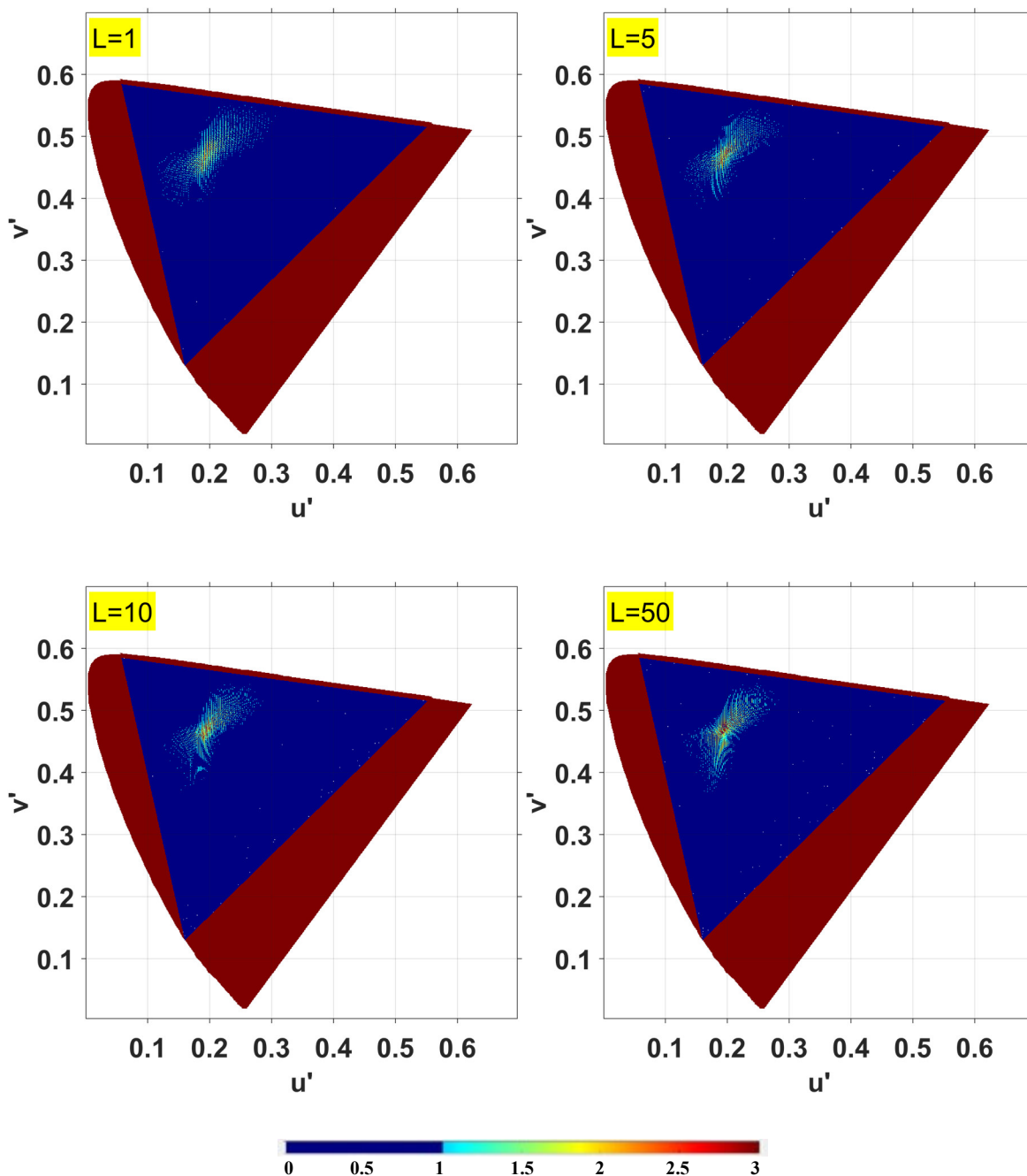
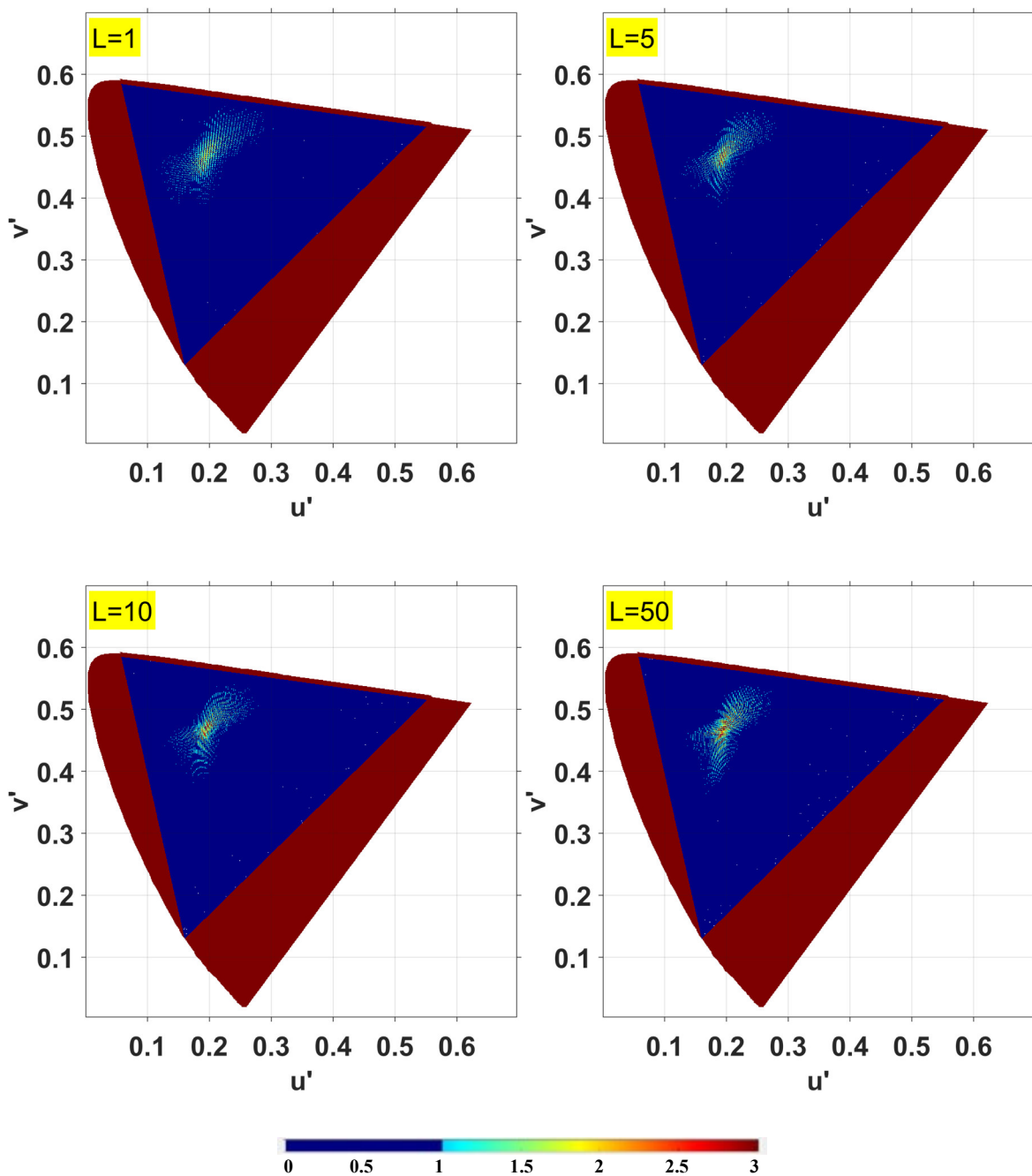
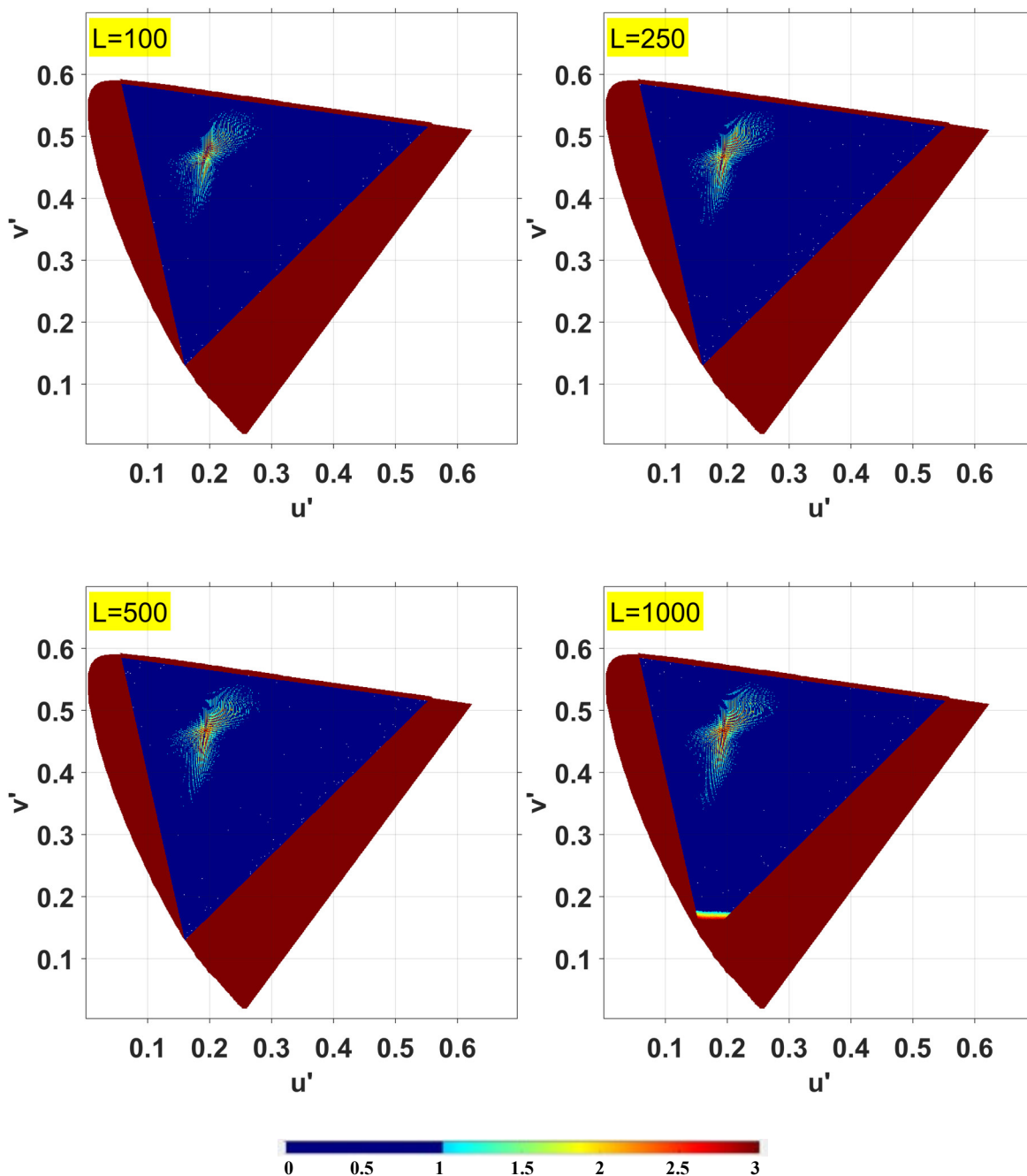


Figure 5.16. Color distortion at different luminance levels (1 to 50  $\text{cd}/\text{m}^2$ ) for 10-bit NCL  $Y_n'$ CBCR with PQ transfer function



**Figure 5.17. Color distortion at different luminance levels (1 to 50 cd/m<sup>2</sup>) for 10-bit our proposed Ya'CBCR with PQ transfer function**



**Figure 5.18. Color distortion at different luminance levels (100 to 1000  $\text{cd}/\text{m}^2$ ) for 10-bit NCL  $Y_n'$ CBCR with PQ transfer function**

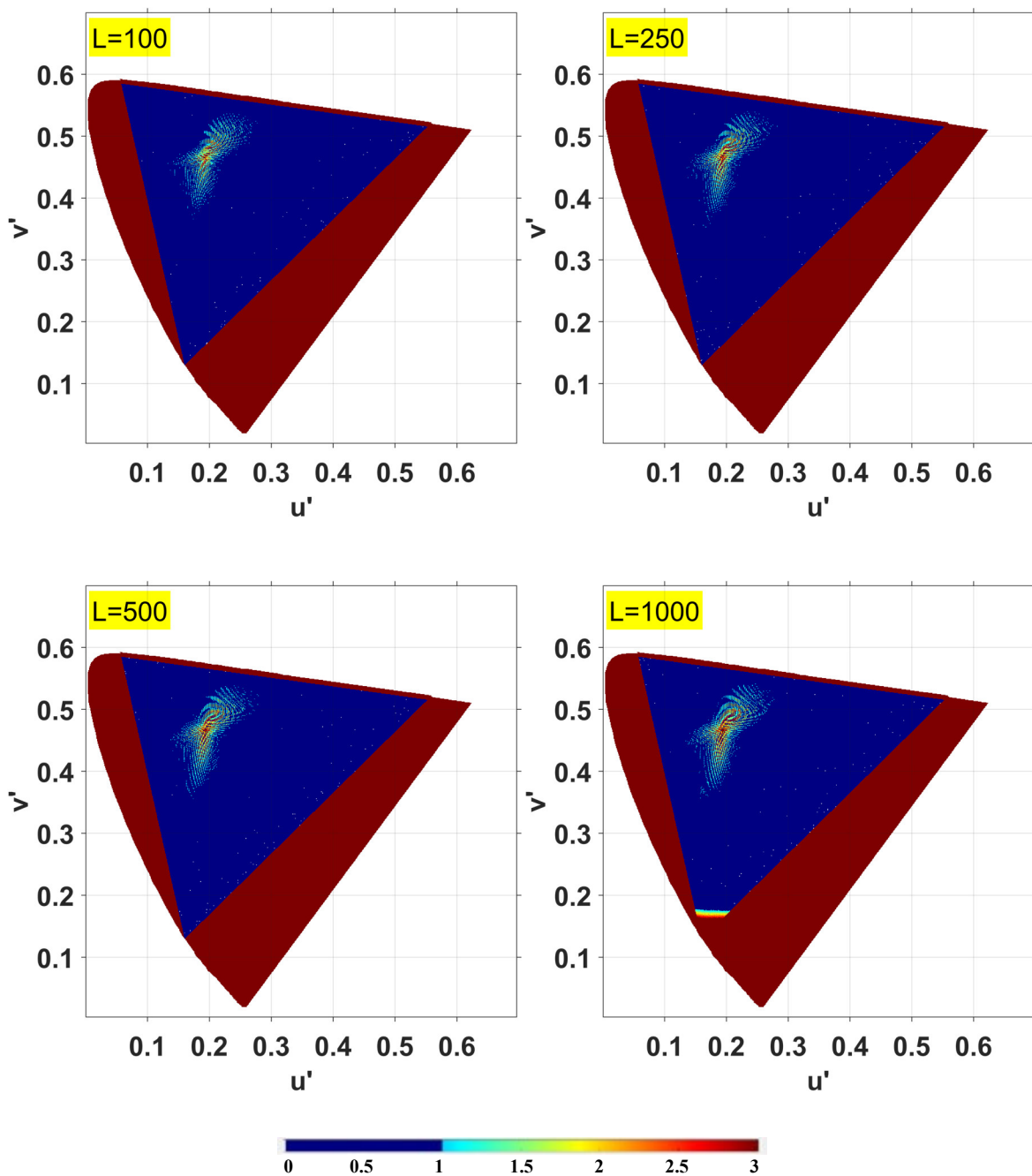


**Figure 5.19. Color distortion at different luminance levels (100 to 1000  $\text{cd}/\text{m}^2$ ) for 10-bit our proposed  $Y_a'$ CBCR with PQ transfer function**

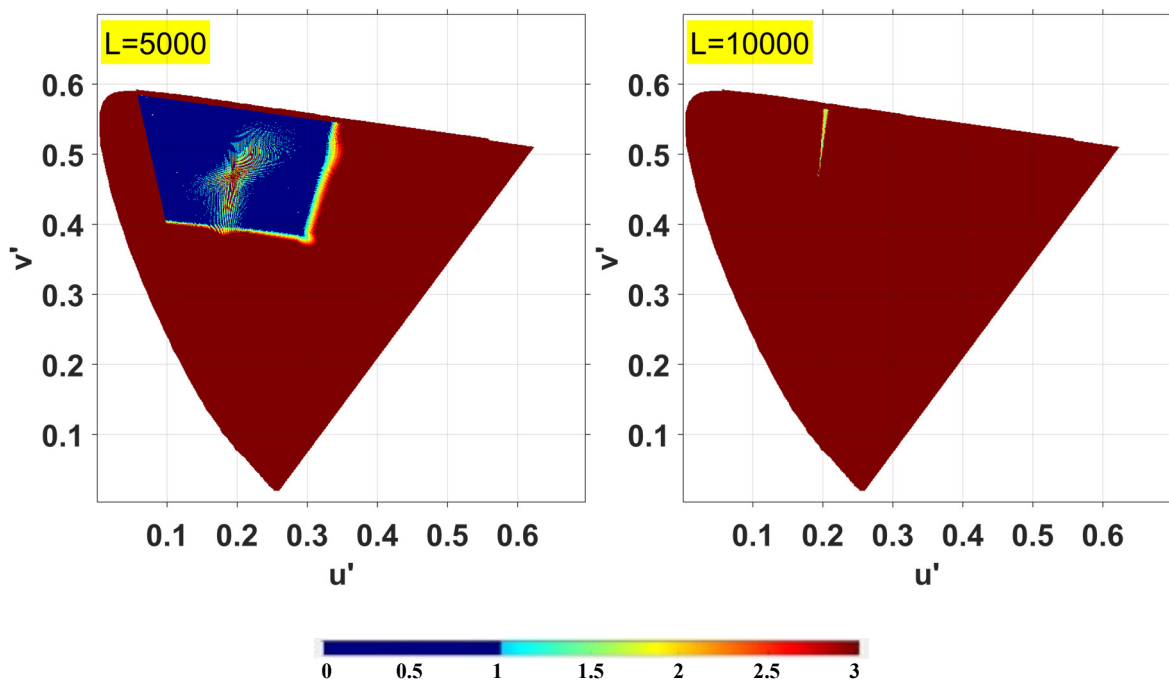


**Figure 5.20. Color distortion at different luminance levels (5000 and 10000  $\text{cd}/\text{m}^2$ ) for 10-bit NCL  $Y_n'B_C B_R$  with PQ transfer function**

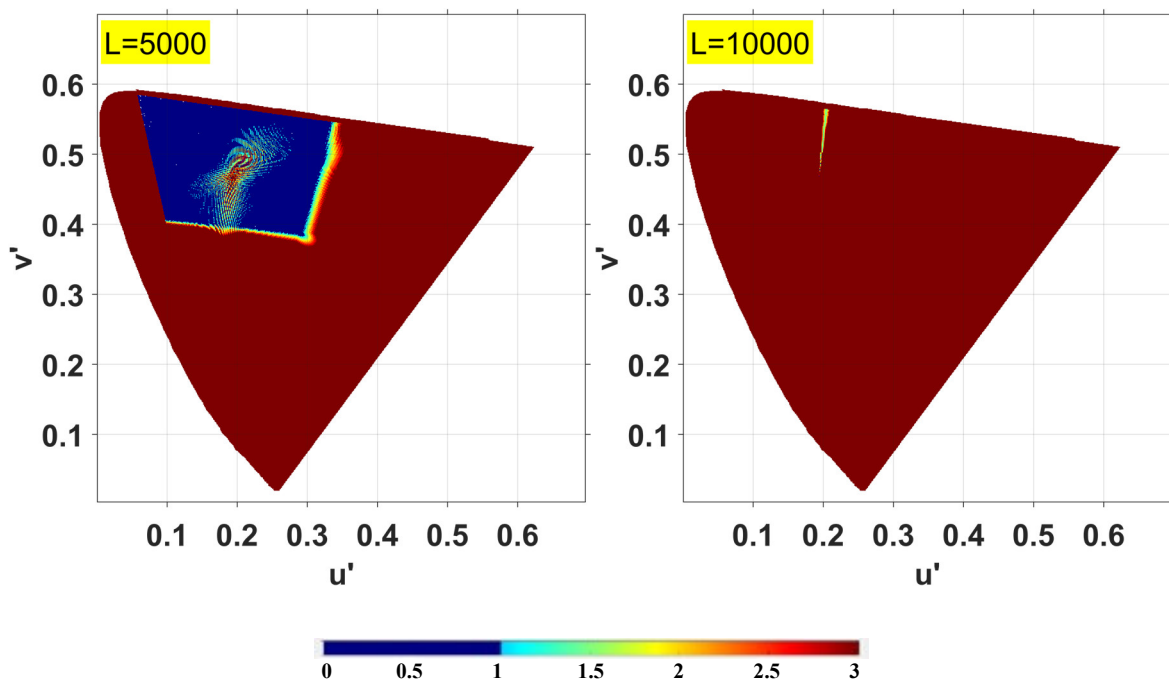


**Figure 5.21. Color distortion at different luminance levels (5000 and 10000  $\text{cd}/\text{m}^2$ ) for 10-bit our proposed  $Y_a'$ CBCR with PQ transfer function**

Comparing the color errors as shown in Figs. 5.14 to 5.21, we observe that our method successfully reduces color distortion over NCL approach at each luminance level. Table 5.5 reports, the max and the average CIEDE2000 values at each luminance level. While the max value is the same for each chosen luminance, our proposed method always produces lower average values (less visible color distortion). Note that since at 0.005 and 10,000  $\text{cd/m}^2$ , there are barely colors visible to human eyes, these two luminance levels are not included in the table. Table 5.6 reports the percentage for CIEDE2000 values less than 1 at each luminance level. Results indicate that our method increases the percentage of values lower than 1, which means an increase in color differences that are not perceptible to our eyes. In other words, our method successfully reduces visible color errors over the NCL approach. All these experiments and observations demonstrate that by changing NCL method with our proposed encoding scheme, color errors are reduced and become less noticeable.

**Table 5.5: Max and average CIEDE2000 values for NCL and our method at each luminance levels**

Luminance level ( $\text{cd/m}^2$ )	NCL max CIEDE2000	Our max CIEDE2000	NCL average CIEDE2000	Our average CIEDE2000
0.01	19.7323	19.7323	0.8660	0.8463
0.05	32.7981	32.7981	1.0021	0.9982
0.1	40.2353	40.2353	0.6309	0.6261
1	106.9007	106.9007	0.9173	0.9152
5	120.0211	120.0211	0.6868	0.6846
10	123.9355	123.9355	0.6549	0.6525
50	130.5879	130.5879	0.6332	0.6298
100	132.6102	132.6102	0.6328	0.6299
250	134.6968	134.6968	0.6385	0.6360
500	135.9149	135.9149	0.6454	0.6426
1000	136.8833	136.8833	0.7388	0.7356
5000	138.2815	138.2815	0.6672	0.6581

**Table 5.6: Percentage of CIEDE2000 values less than one for NCL and our method at each luminance level**

Luminance level (cd/m <sup>2</sup> )	NCL percentage for CIEDE2000 < 1	Our percentage for CIEDE2000 < 1
0.01	70.00%	71.19%
0.05	90.23%	90.65%
0.1	93.93%	94.49%
1	97.41%	97.55%
5	97.88%	98.03%
10	97.85%	97.99%
50	97.48%	97.65%
100	97.32%	97.46%
250	97.04%	97.17%
500	96.76%	96.93%
1000	95.92%	96.15%
5000	87.47%	87.85%

Combining the above-mentioned visual color difference experiment with the compression results reported in Table 5.4, we can conclude that our method increases the color quality compared with NCL approach when using same bit-rate. Furthermore, color distortion for colors at different luminance levels is also reduced by our proposed approach. Most importantly, we preserve the NCL implementation cost by simply switching existing NCL coefficients with our new optimized coefficients. Thus, our method also offers backward compatibility with legacy displays.

## 5.5 Conclusion

In this chapter, we propose a weighted global optimization method that reduces the difference between NCL and CL luma values by prioritizing the importance of RGB colors. Our method separates all colors into three categories, Red, Green, or Blue (three color primaries), by

dividing the CIE 1931 chromaticity diagram into three regions. Different weights for each category are assigned based on their contribution to generated luminance.

Compression evaluations show that our approach reduces bit-rate requirements over the NCL while maintaining same level of color quality. An average of 4.9% bit-rate savings is observed for the same color quality in the CIE  $L^*a^*b^*$  color space [33]. Color errors measured by the CIEDE2000 metric [32] for all possible colors at different luminance levels are also reduced according to our visual color difference experiment. Although our method slightly increases the bit-rate over NCL for the same visual quality in the XYZ color space measured by  $tOSNR$ -XYZ metric, the increase is relatively small (2.23%).

At the decoding end,  $R'G'B'$  values are reconstructed from  $Ya'C_B C_R$  using the newly calculated coefficients for  $R'$ ,  $G'$ ,  $B'$ , and the chroma scaling factors, which are transmitted via an SEI message supported by the HEVC standard.

## 6 Conclusion and Future Work

### 6.1 Conclusion

In this thesis, we investigate the possibility of improving the performance of NCL to the levels offered by CL, aiming at high compression efficiency and color accuracy for HDR content delivery, while maintaining the current SDR pipeline infrastructure.

In Chapter 3, we proposed a global optimization method to approximate NCL values to those of CL. This approach considers all possible RGB combinations with equal importance and derives new set of coefficients for perceptually encoded R'G'B' values that close the gap between NCL and CL values. Compression experiments with HDR sequences were conducted. Results indicate improved visual quality measured by tOSNR-XYZ metric. Compared with the NCL approach, our method reduced bit-rate requirement by an average of 4.74% when preserving same visual quality in the XYZ color space. However, color quality measured by DE100 metric show an average of 20.6% bit-rate increase. The lower color quality is due to the fact that global optimization treats all RGB values as equally important, which is not practical for natural content as their chromaticity distribution does not cover whole gamut. Furthermore, RGB combinations included in the content only occupy a fraction of all possible RGB code values. Thus, the resulted coefficients have been compromised for optimizing pixels that may not exist in the video sequence.

In Chapter 4, we overcome the above-mentioned issues by using a content adaptive optimization method, which takes RGB density of content into consideration and optimizes only these RGB values. Compression results show that our proposed method yields improved color quality for content with one prominent primary (either R, G, or B). For such sequences, an average

of 4.98% bit-rate savings is observed for the same color quality in the CIE L\*a\*b color space [33]. However, similar performance is not observed for uniformly distributed sequences, where our approach results in lower color quality. This is due to the fact that these uniform distributed contents cover more chromaticity range than sequences with prominent red, green, or blue pixels. Thus, adaptive optimization for such content has similar effect as global optimization, which assigns the same importance to all possible RGB values.

Finally, in Chapter 5, we proposed a weighted global optimization method, which separates all colors into three categories, Red, Green, or Blue. Furthermore, we assigned different weights for each category based on their contributions to luminance. Thus, greenish pixels are considered as the most important during the optimization process while blueish pixels have the least significance. After compression tests, we observed an average of 4.9% bit-rate savings for keeping same level of color quality in the CIE L\*a\*b color space [33]. Furthermore, our method successfully reduced color distortions measured by CIEDE2000 metric [32] for all possible colors at each luminance level.

## **6.2 Future Work**

In our experiments, all evaluations are based on objective metrics. A subjective evaluation should be conducted to visually assess the impact of our proposed new color encoding scheme. For this evaluation, however, a prototype HDR display that supports BT.2020 color gamut is needed.

In our compression tests, we prepared the content in the pre-processing stage using our method and then compressed it using the HEVC test model software (HM 16.7). After compression, we applied our approach during the post-processing stage and conducted objective evaluations. Thus, our newly derived coefficients and chroma scaling factors are not transmitted in this entire workflow. Future evaluations of sending new coefficients as metadata to HEVC codec should be performed to more accurately determine the gain/performance of our approach.

## Bibliography

- [1] R. Boitard, M. T. Pourazad, P. Nasiopoulos and J. Slevinsky, "Demystifying High-Dynamic-Range Technology: A new evolution in digital media," *Consumer Electronics Magazine, IEEE*, vol. 4, pp. 72-86, 2015.
- [2] H. Seetzen, W. Heidrich, W. Stuerzlinger, G. Ward, L.-A. Whitehead, M. Trentacoste, A. Ghosh, and A. Vorozcovs, "High dynamic range display systems," *ACM Transactions on Graphics*, vol. 23, pp. 760, 2004.
- [3] Y. Chang, M. Naccari, D. Agrafiotis, M. Mrak, and D. R. Bull, "High Dynamic Range Video Compression Exploiting Luminance Masking," *IEEE Transactions on Circuits and Systems for Video Technology*, vol. 26, no. 5, pp. 950-964, May 2016.
- [4] M. Azimi, R. Boitard, M. T. Pourazad, and P. Nasiopoulos, "Performance Evaluation of Single Layer HDR Video Transmission Pipelines," Submitted to *IEEE Trans. Consum. Electron.*, vol. 62, no. 2.
- [5] ITU, "Recommendation ITU-R BT.2020-2: Parameter values for ultra-high definition television systems for production and international programme exchange," International Telecommunication Union, 2015.
- [6] ITU, "Recommendation ITU-R BT.709-6: Parameter values for the HDTV standards for production and international programme exchange," International Telecommunication Union, 2015.
- [7] B. Belmudez, "Audiovisual Quality Assessment and Prediction for Videotelephony," Switzerland: Springer, 2015.
- [8] ITU, "Report ITU-R BT.2246-5: The present state of ultra-high definition television,"

- International Telecommunication Union, 2015.
- [9] D. Forsyth, and J. Ponce, “Computer vision: A Modern Approach,” Upper Saddle River, NJ, USA: London: Prentice Hall, 2011.
- [10] TS. Sazzad, S. Islam, MM. Mamun, and MZ. Hasan, “Establishment of an Efficient Color Model from Existing Models for Better Gamma Encoding in Image Processing,” *International Journal of Image Processing*, vol. 7, no. 1, pp. 90-100, 2013.
- [11] S. Miller, M. Nezamabadi, and S. Daly, “Perceptual Signal Coding for More Efficient Usage of Bit Codes,” *SMPTE Motion Imaging Journal*, vol. 122, no. 4, pp. 52-59, 2013.
- [12] F. Xie, R. Boitard, M. T. Pourazad, and P. Nasiopoulos, “Optimizing Non Constant Luminance into Constant Luminance for High Dynamic Range Video Distribution, ” in *IEEE International Conference on Acoustics, Speech and Signal Processing (ICASSP)*, New Orleans, USA, March 2017.
- [13] P. Ledda, A. Chalmers, T. Troscianko, and H. Seetzen, “Evaluation of Tone Mapping Operators using a High Dynamic Range Display,” *ACM Transactions on Graphics*, vol. 24, no. 3, pp. 640-648, 2005.
- [14] G. J. Sullivan, J. R. Ohm, W. J. Han, and T. Wiegand, “Overview of the High Efficiency Video Coding (HEVC) standard,” *IEEE Transactions on Circuits and Systems for Video Technology*, vol. 22, no. 12, pp. 1649-1668, 2012.
- [15] J. Samuelsson, “Conversion and Coding Practices for HDR/WCG Video, Draft 1,” in *ISO/IEC JTC1/SC29/WG11 MPEG2016/W1010*, San Diego, USA, Feb. 2016.
- [16] <http://www.cambridgeincolour.com/tutorials/gamma-correction.htm>
- [17] ITU, “Recommendation ITU-R BT.1886: Reference electro-optical transfer function for

- flat panel displays used in HDTV studio production,” International Telecommunication Union, 2011.
- [18] SMPTE, “SMPTE standard ST 2086, Mastering Display Color Volume Metadata Supporting High Luminance and Wide Color Gamut Images,” Society of Motion Pictures Television Engineers, 2014.
- [19] S. Miller, M. Nezamabadi, and S. Daly, “Perceptual Signal Coding for More Efficient Usage of Bit Codes,” SMPTE Motion Imaging Journal, vol. 122, no. 4, pp. 52–59, May 2013.
- [20] R. Boitard, R. K. Mantiuk, and T. Pouli, “Evaluation of Color Encodings for High Dynamic Range Pixels,” in Proc. SPIE, vol. 9394, Human Vision and Electronic Imaging XX, San Francisco, March 2015.
- [21] A. Luthra, E. Francois, and W. Husak, “Call for Evidence (CfE) for HDR and WCG Video Coding,” in ISO/IEC JTC1/SC29/WG11 MPEG2015/N15083. Geneva, Switzerland, Feb. 2015.
- [22] <https://www.willamette.edu/~gorr/classes/GeneralGraphics/Color/tristimulus.htm>
- [23] E. Reinhard, W. Heidrich, P. Debevec, S. Pattanaik, G. Ward, and K. Myszkowski, “High Dynamic Range Imaging: Acquisition, Display, and Image-based Lighting,” Burlington, MA, USA: Morgan Kaufmann, 2010.
- [24] D. A. Kerr, “The CIE XYZ and xyY Color Spaces,” Colorimetry, vol. 1, no. 1, pp. 1 – 16, 2010.
- [25] ITU, “Report ITU-R BT.2390-0: High dynamic range television for production and international programme exchange,” International Telecommunication Union, 2016.

- [26] S. Y. Choi, K. J. Oh, D. S. Park, and D. K. Nam, “Constant vs. Non-constant Luminance Video Signals for UHD TV,” SID Symposium Digest of Technical Papers, vol. 44, no. 1, pp. 26, 2013.
- [27] J. Strom, J. Samuelsson, and K. Dovstam, “Luma Adjustment for High Dynamic Range Video,” Data Compression Conference (DCC), pp. 319 – 328, 2016.
- [28] A. Norkin, “Fast Algorithm for HDR Color Conversion,” Data Compression Conference (DCC), pp. 486 – 495, 2016.
- [29] V. Sze, M. Budagavi, and G. J. Sullivan, “High efficiency Video Coding (HEVC),” Integrated Circuit and Systems, Algorithms and Architectures, Switzerland: Springer, 2014.
- [30] <https://hevc.hhi.fraunhofer.de/>
- [31] A. M. Tourapis, and D. Singer, “HDRTools: Software Updates,” in ISO/IEC JTC1/SC29/WG11 MPEG2015/M35797. Geneva, Switzerland, Feb. 2015.
- [32] S. Gaurav, W. Wu, and E. N. Dalal, “The CIEDE2000 Color-Difference Formula: Implementation Notes, Supplementary Test Data, and Mathematical Observations,” Color Research & Application, vol. 30, no. 1, pp. 21-30, 2005.
- [33] G. Wyszecki, and W. S. Stiles, *Color science: Concepts and Methods, Quantitative Data and Formulae*, New York, NY, USA: Wiley, 1982.
- [34] G. Bjontegaard, “Calculation of Average PSNR Difference between RD Curves,” in Proc. 13<sup>th</sup> Meeting ITU-T Q.6/SG16 VCEG, April. 2001.

- [35] D. Touze, and E. Francois, "Description of new version of class A sequences provided by Technicolor," in ISO/IEC JTC1/SC29/WG11 MPEG2015/M35477. Geneva, Switzerland, Feb. 2015.
- [36] D. Malas, R. Bleuten, E. Francois, K. Minoo, and E. Alshina, "CableLabs HDR Content Usage," in ISO/IEC JTC1/SC29/WG11 MPEG2015/M35465. Geneva, Switzerland, Feb. 2015.
- [37] Y. Thomas, "Conditions of use of EBU Zurich Athletics material," in ISO/IEC JTC1/SC29/WG11 MPEG2015/M36666. Warsaw, Poland, June. 2015.
- [38] K. Suehring, K. Sharman, A. Tourapis, "JCT-VC AHG report: HEVC HM and HDRTTools software development and software technical evaluation (AHG3)," in ISO/IEC JTC1/SC29/WG11 MPEG2017/M40098. Geneva, Switzerland, Jan. 2017.
- [39] <https://www.wou.edu/las/physci/ch462/tmcolors.htm>
- [40] <http://hyperphysics.phy-astr.gsu.edu/hbase/vision/specol.html>
- [41] Unknown Author, "LED Color Mixing: Basics and Background," Technical Article, CLD-AP38, Revision 1, 2010.
- [42] E. Francois, C. Fogg, Y. He, X. Li, A. Luthra, and C. Segall, "High Dynamic Range and Wide Color Gamut Video Coding in HEVC: Status and Potential Future Enhancements," IEEE Transactions on Circuits and Systems for Video Technology, vol. 26, no. 1, pp. 63–75, Jan. 2016.
- [43] T. Wiegand, G. J. Sullivan, G. Bjontegaard and A. Luthra, "Overview of the H.264/AVC video coding standard," IEEE Transactions on Circuits and Systems for Video Technology, vol. 13, pp. 560-576, 2003.

- [44] IITU, “Recommendation ITU-R BT.2100-0: Image parameter values for high dynamic range television for use in production and international programme exchange,” International Telecommunication Union, 2016.
- [45] T. Lu, F. Pu, P. Yin, T. Chen, W. Husak, J. Pytlarz, R. Atkins, J. Frohlich, and G. M. Su, “ITP Color Space and its Compression Performance for High Dynamic Range and Wide Color Gamut Video Distribution,” ZTE Communications, vol. 14, no. 1, pp. 32-38, 2016.
- [46] M. Azimi, R. Boitard, M. T. Pourazad, and P. Nasiopoulos, “Visual Color Difference Evaluation of Standard Color Pixel Representations for High Dynamic Range Video Compression,” submitted to European Signal Processing Conference (EUSIPCO), 2017.
- [47] M. Singha, and K. Hemachandran, “Performance Analysis of Color Spaces in Image Retrieval,” Assam University Journal of Science and Technology, vol. 7, no. 2, pp. 94-104, 2011.
- [48] M. Tkalcic, and J. F. Tasic, “Colour Spaces – Perceptual, Historical and Applicational Background,” IEEE, vol. 1, pp. 304-308, 2003.
- [49] G. W. Larson, “LogLuv Encoding for Full-Gamut, High-Dynamic Range Images,” Journal of Graphics Tools, vol. 3, no.1, pp. 15-31, 1998.
- [50] L. Lucchese, S. K. Mitra, and J. Mukherjee, “A New Algorithm Based on Saturation and Desaturation in the xy Chromaticity Diagram for Enhancement and Re-Rendition of Color Images,” in IEEE International Conference on Image Processing, vol. 2, pp. 1077-1080, 2001.
- [51] [http://www.centasiathai.com/wp-content/uploads/2016/03/RES-224\\_Display-White-Point.pdf](http://www.centasiathai.com/wp-content/uploads/2016/03/RES-224_Display-White-Point.pdf)